Theoretical issues

S. Moch, M. Rogal, J. A. M. Vermaseren, A. Vogt, G. Altarelli, R. D. Ball, M. Ciafaloni, D. Colferai, S. Forte, G. P. Salam, A. Staśto, R. S. Thorne, C. D. White, G. Beuf, F. Caola, F. Gelis, L. Motyka, C. Royon, D. Šálek, A. M. Staśto

1 Precision calculations for inclusive DIS: an update[1]

With high-precision data from HERA and in view of the outstanding importance of hard scattering cross sections at the LHC, a quantitative understanding of deep-inelastic processes is indispensable, necessitating calculations beyond the standard next-to-leading order of perturbative QCD.

In this contribution we briefly discuss the recent extension of the three-loop calculations for inclusive deep-inelastic scattering (DIS) [1–8] to the complete set of coefficient functions for the charged-current (CC) case. The new third-order expressions are too lengthy for this short overview. They can be found in Refs. [9, 10] together with the calculational methods and a more detailed discussion. Furthermore the reader is referred to Refs. [11, 12] for our first results on the three-loop splitting functions for the evolution of helicity-dependent parton distributions.

Structure functions in inclusive deep-inelastic scattering are among the most extensively measured observables. The combined data from fixed-target experiments and the HERA collider spans about four orders of magnitude in both Bjorken-x variable and the scale $Q^2 = -q^2$ given by the momentum q of the exchanged electroweak gauge boson [13]. Here we consider the W-exchange charged-current case, see Refs. [14–20] for recent data from neutrino DIS and HERA. With six structure functions, $F_2^{W^\pm}$, $F_3^{W^\pm}$ and $F_L^{W^\pm}$, this case has a far richer structure than, for example, electromagnetic DIS with only two independent observables, F_2 and F_L.

Even taking into account a forthcoming combined H1/ZEUS final high-Q^2 data set from HERA, more detailed measurements are required to fully exploit the resulting potential, for instance at a future neutrino factory, see Ref. [21], and the LHeC, the proposed high-luminosity electron-proton collider at the LHC [22]. Already now, however, CC DIS provides important information on the parton structure of the proton, e.g., its flavour decomposition and the valence-quark distributions. Moreover, present results are also sensitive to electroweak parameters of the Standard Model such as $\sin^2\theta_W$, see Ref. [23], and the space-like W-boson propagator [24]. As discussed, for example, in Refs. [25–28], a reliable determination of $\sin^2\theta_W$ from neutrino DIS requires a detailed understanding of non-perturbative and perturbative QCD effects.

Previous complete results on unpolarized DIS include the three-loop splitting functions [4, 5] as well as the 3-loop coefficient functions for the photon-exchange structure functions $F_{2,L}$ [6, 7]. However, most coefficient functions for CC DIS were not fully computed to three loops so far.

For this case it is convenient to consider linear combinations of the structure functions $F_a^{W^\pm}$ with simple properties under crossing, such as $F_a^{\nu p \pm \bar{\nu} p}$ ($a = 2,\ 3,\ L$) for neutrino DIS.

[1] Contributing authors: S. Moch, M. Rogal, J. A. M. Vermaseren, A. Vogt

For all these combinations either the even or odd moments can be calculated in Mellin-N space in the framework of the operator product expansion (OPE), see Ref. [29]. The results for the third-order coefficient functions for the even-N combinations $F_{2,L}^{\nu p+\bar{\nu}p}$ can be taken over from electromagnetic DIS [6, 7]. Also the coefficient function for the odd-N based charged-current structure function $F_3^{\nu p+\bar{\nu}p}$ is completely known at three-loop accuracy, with the results only published via compact parameterizations so far [8]. For the remaining combinations $F_{2,L}^{\nu p-\bar{\nu}p}$ and $F_3^{\nu p-\bar{\nu}p}$, on the other hand, only recently the first six odd or even integer moments of the respective coefficient functions have been calculated to third order in Ref. [9] following the approach of Refs. [1–3] based on the MINCER program [30, 31].

The complete results of Refs. [6–8] fix all even and odd moments N. Hence already the present knowledge of fixed Mellin moments for $F_{2,L}^{\nu p-\bar{\nu}p}$ and $F_3^{\nu p-\bar{\nu}p}$ is sufficient to determine also the lowest six moments of the differences of corresponding even-N and odd-N coefficient functions and to address a theoretical conjecture [32] for these quantities, see Ref. [10]. Furthermore these moments facilitate x-space approximations in the style of, e.g, Ref. [33] which are sufficient for most phenomenological purposes, including the determination of the third-order QCD corrections to the Paschos-Wolfenstein relation [34] used for the extraction of $\sin^2\theta_W$ from neutrino DIS.

The even-odd differences of the CC coefficient functions C_a for $a = 2,\ 3,\ L$ can be defined by

$$\delta\, C_{2,L} \ = \ C_{2,L}^{\nu p+\bar{\nu}p} - C_{2,L}^{\nu p-\bar{\nu}p} \ , \qquad \delta\, C_3 \ = \ C_3^{\nu p-\bar{\nu}p} - C_3^{\nu p+\bar{\nu}p} \ . \tag{1}$$

The signs are chosen such that the differences are always 'even – odd' in the moments N accessible by the OPE [29], and it is understood that the $d^{abc}d_{abc}$ part of $C_3^{\nu p+\bar{\nu}p}$ [3, 8] is removed before the difference is formed. With $a_{\rm s} = \alpha_{\rm s}/(4\pi)$ these non-singlet quantities can be expanded as

$$\delta\, C_a \ = \ \sum_{l=2} a_{\rm s}^{\,l}\ \delta c_a^{(l)}. \tag{2}$$

There are no first-order contributions to these differences, hence the above sums start at $l = 2$.

We start the illustration of these recent results by looking at the approximations for the $\nu p - \bar{\nu} p$ odd-N coefficient functions $c_{2,L}^{(3)}(x)$ (see Ref. [10] for a detailed discussion). These are compared in Fig. 1 to their exact counterparts [6, 7] for the even-N non-singlet structure functions. The dashed lines represent the uncertainty band due to the limited number of known moments. The third-order even-odd differences remain noticeable to larger values of x than at two loops, e.g., up to $x \simeq 0.3$ for F_2 and $x \simeq 0.6$ for F_L for the four-flavour case shown in the figure. The moments $N = 1,\ 3,\ \ldots,\ 9$ constrain $\delta\, c_{2,L}^{(3)}(x)$ very well at $x \gtrsim 0.1$, and approximately down to $x \approx 10^{-2}$.

Concerning low values of Bjorken-x one should recall that the uncertainty bands shown by the dashed lines in Fig. 1 do not directly indicate the range of applicability of these approximations, since the coefficient functions enter observables only via smoothening Mellin convolutions with non-perturbative initial distributions. In Fig. 2 we therefore present the convolutions of all six third-order CC coefficient functions with a characteristic reference distribution. It turns

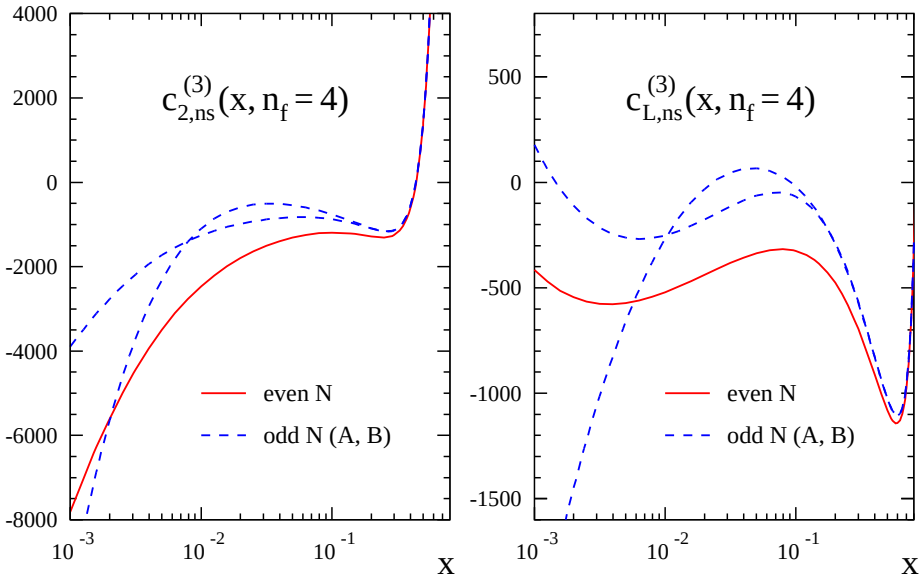

Fig. 1: The exact third-order coefficient functions of the even-N structure functions $F_{2,L}^{\nu p+\bar{\nu}p}$ for four massless flavours, and the approximate odd-moment quantities for $\nu p - \bar{\nu} p$ combination.

out that the approximations of the previous figure can be sufficient down to values even below $x = 10^{-3}$, which is amply sufficient for foreseeable applications to data. The uncertainty of $\delta c_3^{(3)}(x)$, on the other hand, becomes relevant already at larger values, $x \lesssim 10^{-2}$, as the lowest calculated moment of this quantity, $N = 2$, has far less sensitivity to the behaviour at low x.

The three-loop corrections to the non-singlet structure functions are rather small even well below the x-values shown in the figure – recall our small expansion parameter a_s: the third-order coefficient are smaller by a factor $2.0 \cdot 10^{-3}$ if the expansion is written in powers of α_s. Their sharp rise for $x \to 1$ is understood in terms of soft-gluon effects which can be effectively resummed, if required, to next-to-next-to-next-to-leading logarithmic accuracy [35]. Our even-odd differences $\delta c_a^{(3)}(x)$, on the other hand, are irrelevant at $x > 0.1$ but have a sizeable impact at smaller x in particular on the corrections for F_2 and F_L. The approximate results for $\delta c_a^{(3)}(x)$ facilitate a first assessment of the perturbative stability of the even-odd differences (1). In Fig. 3 we illustrate the known two orders for F_2 and F_L for $\alpha_s = 0.25$ and $n_f = 4$ massless quark flavours, employing the same reference quark distribution as in Fig. 2.

Obviously our new α_s^3 corrections are important wherever these coefficient-function differences are non-negligible. On the other hand, our results confirm that these quantities are very small, and thus relevant only when a high accuracy is required. These conditions are fulfilled for the calculation of QCD corrections for the so-called Paschos-Wolfenstein relation. This relation is defined in terms of a ratio of neutral-current and charged-current cross sections for neutrino-nucleon DIS [34],

$$R^- \;=\; \frac{\sigma(\nu_\mu N \to \nu_\mu X) \;-\; \sigma(\bar{\nu}_\mu N \to \bar{\nu}_\mu X)}{\sigma(\nu_\mu N \to \mu^- X) \;-\; \sigma(\bar{\nu}_\mu N \to \mu^+ X)} \;. \tag{3}$$

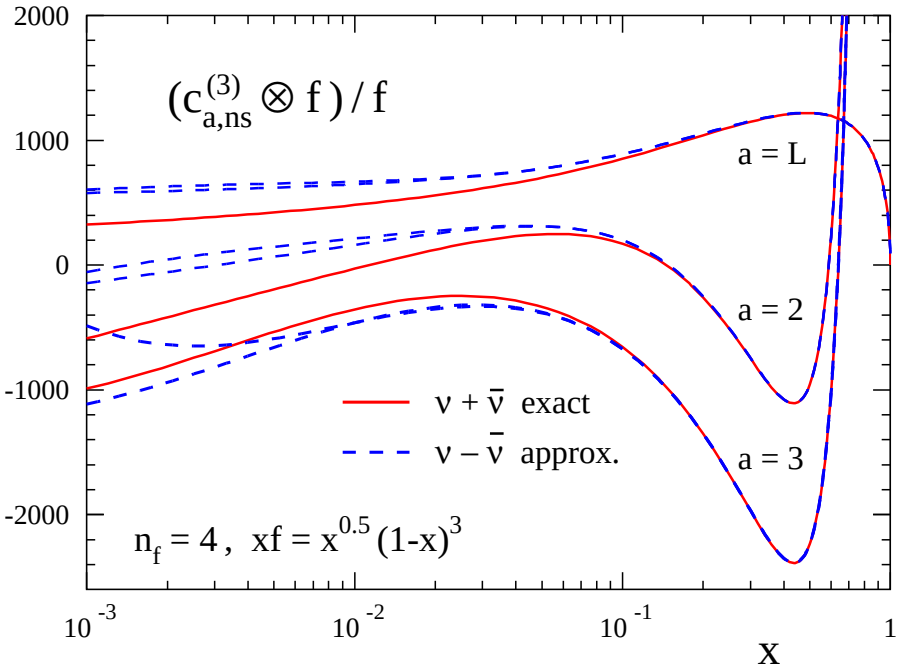

Fig. 2: Convolution of the six third-order CC coefficient functions for $F_{2,3,L}$ in $\nu p + \bar{\nu} p$ and $\nu p - \bar{\nu} p$ DIS with a schematic but typical non-singlet distribution f. All results have been normalized to $f(x)$, suppressing the large but trivial variation of the absolute convolutions.

The asymmetry R^- directly measures $\sin^2\theta_W$ if the up and down valence quarks in the target carry equal momenta, and if the strange and heavy-quark sea distributions are charge symmetric. Beyond the leading order this asymmetry can be presented as an expansion in α_s and inverse powers of the dominant isoscalar combination $u^- + d^-$, where $q^- = \int_0^1 dx\; x\,(q(x) - \bar{q}(x))$ is the second Mellin moment of the valence quark distributions. Using the results for differences $\delta c_a^{(3)}(x), a = 2, L, 3$ one can present it in a numeric form,

$$R^- \;=\; \frac{1}{2} - \sin^2\theta_W \;+\; \frac{u^- - d^- + c^- - s^-}{u^- + d^-} \left\{ 1 - \frac{7}{3}\,\sin^2\theta_W \;+\; \left(\frac{1}{2} - \sin^2\theta_W\right) \cdot \right.$$
$$\left. \frac{8}{9}\frac{\alpha_s}{\pi}\left[\,1 + 1.689\,\alpha_s + (3.661 \pm 0.002)\,\alpha_s^2\,\right] \right\} \;+\; \mathcal{O}\left((u^- + d^-)^{-2}\right) \;+\; \mathcal{O}\left(\alpha_s^4\right) \;, \quad (4)$$

where the third term in the square brackets is determined by the α_s^3 corrections $\delta c_a^{(3)}(x), a = 2, L, 3$. The perturbation series in the square brackets appears reasonably well convergent for relevant values of the strong coupling constant, with the known terms reading, e.g., 1 + 0.42 + 0.23 for $\alpha_s = 0.25$. Thus the α_s^2 and α_s^3 contributions correct the NLO estimate by 65% in this case. On the other hand, due to the small prefactor of this expansion, the new third-order term increases the complete curly bracket in Eq. (4) by only about 1%, which can therefore by considered as the new uncertainty of this quantity due to the truncation of the perturbative expansion. Consequently previous NLO estimates of the effect of, for instance, the (presumably

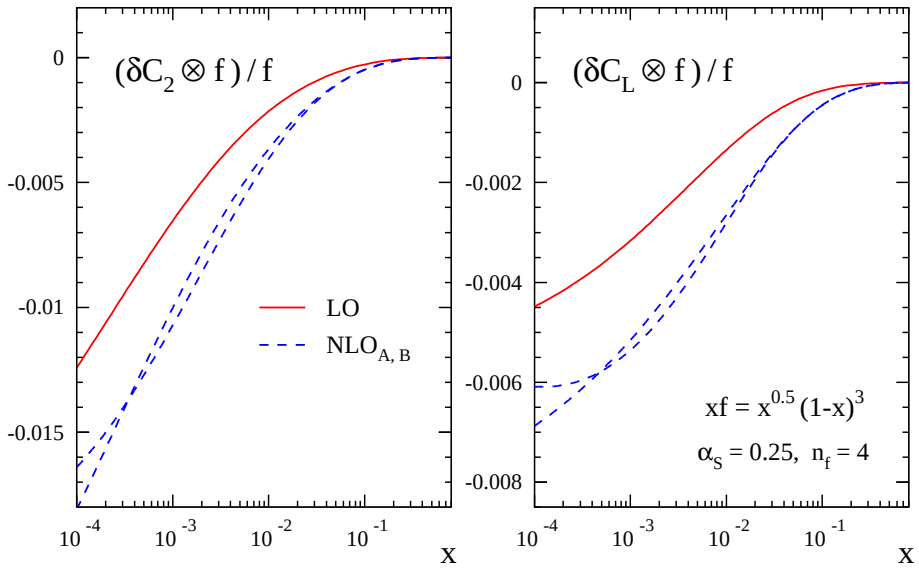

Fig. 3: The first two approximations, denoted by LO and NLO, of the differences (1) for F_2 and F_L in charged-current DIS. The results are shown for representative values of α_s and n_f after convolution with the reference distribution $f(x)$ also employed in Fig. 2. The dashed curves correspond to the two approximation uncertainties for the new α_s^3 contributions.

mainly non-perturbative, see Refs. [36–38]) charge asymmetry of the strange sea remain practically unaffected by higher-order corrections to the coefficient functions.

To summarize, we have extended the fixed-N three-loop calculations of inclusive DIS [1–3] to all charged-current cases not covered by the full (all-N) computations of Refs. [6–8]. The region of applicability of these new results is restricted to Bjorken-x values above about 10^{-3}, a range amply sufficiently for any fixed-target or collider measurements of those charged-current structure functions in the foreseeable future. Except for the longitudinal structure function F_L, the present coefficient functions are part of the next-to-next-to-next-to-leading order (N^{3}LO) approximation of massless perturbative QCD. Analyses at this order are possible outside the small-x region since the corresponding four-loop splitting functions will have a very small impact here, cf. Ref. [39].

2 Small x resummation [2]

The splitting functions which govern the evolution of the parton distributions (PDFs), together with the hard cross sections which relate those partons to hadronic physical observables, are potentially unstable at high energy due to logarithmically enhanced contributions. In particular, parametrizing observables such as deep-inelastic structure (DIS) functions or Drell-Yan (DY) or Higgs production cross section in hadronic collisions in terms of a dimensionful scale Q^2 (photon virtuality or invariant mass of the final state in DIS and DY respectively) and a dimensionless ratio

[2] Contributing authors: G. Altarelli, R. D. Ball, M. Ciafaloni, D. Colferai, S. Forte, G. P. Salam, A. Staśto, R. S. Thorne, C. D. White

x (the Bjorken variable or $\frac{Q^2}{s}$ in DIS and DY respectively), when $x \to 0$ there are logarithmically enhanced contributions to the perturbation expansion of the form $x^{-1}\alpha_S^n(Q^2)\log^m(1/x)$ ($n \geq m-1$). When x is sufficiently small, one must resum such terms, reordering the perturbation expansion in terms of leading logarithmic (LL) terms followed by next-to-leading logarithmic (NLL) terms and so on.

The problem can be traced to ladders of t-channel gluon exchanges at LL order, with some quark mixing at NLL order and beyond. The underlying framework for the resummation procedure is the BFKL equation [40, 41], an integral equation for the unintegrated gluon $f(k^2, Q_0^2)$ that is currently known up to full NLL order [42–44], and approximate NNLL order [45]. This has the schematic form (up to NLL):

$$Nf(k^2,Q_0^2) = Nf_I(Q_0^2) + \bar{\alpha}_S(k^2)\int dk'^2 \left[\mathcal{K}_0(k^2,k'^2,Q_0^2) + \bar{\alpha}_S(k^2)\mathcal{K}_1(k^2,k'^2,Q_0^2)\right] f(k'^2), \tag{5}$$

where $f_I(Q_0^2)$ is a non-perturbative initial condition at some initial scale Q_0, $\bar{\alpha}_S = 3\alpha_S/\pi$ and $\mathcal{K}_{0,1}$ are the LL and NLL BFKL kernels. Different choices for the argument of the running coupling are possible, leading to accordingly modified $\mathcal{K}_1$ [46, 47].

The solution of the BFKL equation can be used to extract leading and subleading singular contributions to singlet DGLAP splitting functions. The BFKL equation can either be solved numerically in its form given by Eq. (5), or else analytically by performing a double Mellin transform with respect to x and k^2:

$$f(\gamma, N) = \int_0^\infty (k^2)^{-\gamma-1}\int_0^1 dx x^N f(x,k^2), \tag{6}$$

whereby the BFKL equation becomes a differential equation, with kernels $\chi_{0,1}(\gamma)$ defined respectively as the Mellin transforms of $\mathcal{K}_{0,1}$. Furthermore, by using the k_t-factorisation theorem [48], one may determine leading small x contributions to all orders to hard partonic cross sections for physical processes such as heavy quark electroproduction [48] and deep-inelastic scattering [49]. Approximate subleading results are also available [50, 51].

These results for splitting functions and hard partonic cross sections can then be combined with fixed-order results to obtain resummed predictions for physical observables. However, it has now been known for some time that the LL BFKL equation is unable to describe scattering data well, even when matched to a fixed order expansion. Any viable resummation procedure must then, at the very least, satisfy the following requirements:

1. Include a stable solution to the BFKL equation with running coupling up to NLL order.
2. Match to the standard DGLAP description at moderate and high x values (where this is known to describe data well).
3. Provide the complete set of splitting and coefficient functions for F_2 and F_L in a well defined factorisation scheme.

Over the past few years, three approaches have emerged which, to some extent, aim at fulfilling these conditions. Here we call these the ABF [52–59], CCSS [47, 60–66] and TW [67–72] approaches. In the ABF scheme all three requirements are met, and resummed splitting functions in the singlet sector have been determined. Furthermore, a complete control of the

scheme dependence at the resummed level has been achieved, thereby allowing for a consistent determination of resummed deep-inelastic coefficient functions, and thus of resummed structure functions. However, the results obtained thus have not been fit to the data yet. In the CCSS formalism, resummed splitting functions have also been determined. However, results are given in a scheme which differs from the $\overline{\rm MS}$ scheme at the resummed level; furthermore, resummed coefficient functions and physical observables haven't been constructed yet. The TW approach, instead, has already been compared to the data in a global fit. However, this approach makes a number of simplifying assumptions and the ensuing resummation is thus not as complete as that which obtains in other approaches: for example, this approach does not include the full collinear resummation of the BFKL kernel.

A comparison of resummed splitting functions and solution of evolution equations determined in the ABF and CCSS approaches with $n_f = 0$ was presented in Ref. [73]; the main features and differences of these approaches were also discussed. Here, we extend this comparison to the case of $n_f \neq 0$ resummation, and also to the TW approach. First, we will briefly summarize the main features of each approach, and in particular we display the matrix of splitting functions determined in the ABF and CCSS approaches. Then, we will compare K-factors for physical observables determined using the ABF and TW approach.

Note that there are some difference in notations between various groups, which are retained here in order to simplify comparison to the original literature. In particular, the variable N in Eq. (6) will be referred to as ω in the CCS approach of Section 2.2, and the variable γ in the same equation will be referred to as M in the ABF approach of Section 2.1.

2.1 The Altarelli-Ball-Forte (ABF) Approach

In the ABF approach [52–59, 74–77] one concentrates on the problem of obtaining an improved anomalous dimension (splitting function) for DIS which reduces to the ordinary perturbative result at large N (large x), thereby automatically satisfying renormalization group constraints, while including resummed BFKL corrections at small N (small x), determined through the renormalization-group improved (i.e. running coupling) version of the BFKL kernel. The ordinary perturbative result for the singlet anomalous dimension is given by:

$$\gamma(N, \alpha_s) = \alpha_s \gamma_0(N) \; + \; \alpha_s^2 \gamma_1(N) \; + \; \alpha_s^3 \gamma_2(N) \; \ldots . \tag{7}$$

The BFKL corrections at small N (small x) are determined by the BFKL kernel $\chi(M, \alpha_s)$:

$$\chi(M, \alpha_s) = \alpha_s \chi_0(M) \; + \; \alpha_s^2 \chi_1(M) \; + \; \ldots , \tag{8}$$

which is the Mellin transform, with respect to $t = \ln \frac{k^2}{k_0^2}$, of the $N \to 0$ angular averaged BFKL kernel.

The ABF construction is based on three ingredients.

1. *The duality relation* between the kernels χ and γ

$$\chi(\gamma(N, \alpha_s), \alpha_s) = N, \tag{9}$$

which is a consequence of the fact that at fixed coupling the solutions of the BFKL and DGLAP equations should coincide at leading twist [52, 74, 78]. By using duality, one

can use the perturbative expansions of γ and χ in powers of α_s to improve (resum) each other: by combining them, one obtains a "double leading" (DL) expansion which includes all leading (and subleading, at NLO) logs of x and Q^2. In particular, the DL expansion automatically resums the collinear poles of χ at $M = 0$. This eliminates the alternating sign poles $+1/M, -1/M^2, ...$ that appear in χ_0, χ_1,..., and make the perturbative expansion of χ unreliable. This result is a model independent consequence of momentum conservation $\gamma(1, \alpha_s) = 0$, whence, by duality:

$$\chi(0, \alpha_s) = 1. \tag{10}$$

2. *The symmetry of the BFKL kernel* upon gluon interchange. In Mellin space, this symmetry implies that at the fixed-coupling level the kernel χ for evolution in $\ln \frac{s}{kk_0}$ must satisfy $\chi(M) = \chi(1 - M)$. By exploiting this symmetry, one can use the collinear resummation of the region $M \sim 0$ which was obtained using the double-leading expansion to also improve the BFKL kernel in the anti–collinear $M \simeq 1$ region. This leads to a symmetric kernel which is an entire function for all M, and has a minimum at $M = \frac{1}{2}$. The symmetry is broken by the DIS choice of variables $\ln \frac{1}{x} = \ln \frac{s}{Q^2}$ and by the running of the coupling; however these symmetry breaking contribution can be determined exactly. This then leads to a stable resummed expansion of the resummed anomalous dimension at the fixed coupling level.
3. *The running-coupling resummation* of the BFKL solution. Whereas running coupling corrections to evolution equations are automatically included when solving the DGLAP evolution equation with resummed anomalous dimensions, the duality relation Eq. (9) itself undergoes corrections when the running coupling is included in the BFKL equation (5). Running coupling corrections can then be derived order by order, and turn out to be affected by singularities in Mellin M space. This implies that after Mellin inversion the associate splitting functions is enhanced as $x \to 0$: their contribution grows as $\left(\alpha_s \beta_0 \ln \frac{1}{x}\right)^n$ with the perturbative order. However the series of leading enhanced contribution can be summed at all orders in closed form, because it corresponds to the asymptotic expansion in powers of α_s of the solution to the running coupling BFKL equation (5) when the kernel χ is approximated quadratically about its minimum. This exact solution can be expressed in terms of Airy functions [53, 79] when the kernel is linear in α_s and in terms of Bateman [55] functions for generic kernels. Because both the exact solution and its asymptotic expansion are known, this BFKL running coupling resummation can be combined with the DGLAP anomalous dimension, already resummed at the BFKL fixed coupling level, with full control of overlap (double counting terms). Schematically, the result has the following form:

$$\begin{aligned}\gamma^{rc}_{\Sigma\, NLO}(\alpha_{\rm s}(t), N) = \gamma^{rc,pert}_{\Sigma\, NLO}(\alpha_{\rm s}(t), N) + \gamma^B(\alpha_{\rm s}(t), N) - \gamma^B_s(\alpha_{\rm s}(t), N) \\ -\gamma^B_{ss}(\alpha_{\rm s}(t), N) - \gamma^B_{ss,0}(\alpha_{\rm s}(t), N) + \gamma_{\rm match}(\alpha_{\rm s}(t), N) + \gamma_{\rm mom}(\alpha_{\rm s}(t), N),\end{aligned} \tag{11}$$

where $\gamma^{rc,pert}_{\Sigma\, NLO}(\alpha_{\rm s}(t), N)$ contains all terms which are up to NLO in the double-leading expansion of point 1, symmetrized as discussed in point 2 above so that its dual χ has a minimum; $\gamma^B(\alpha_{\rm s}(t), N)$ resums the series of singular running coupling corrections using the aforementioned exact BFKL solution in terms of a Bateman function; $\gamma^B_s(\alpha_{\rm s}(t), N)$,

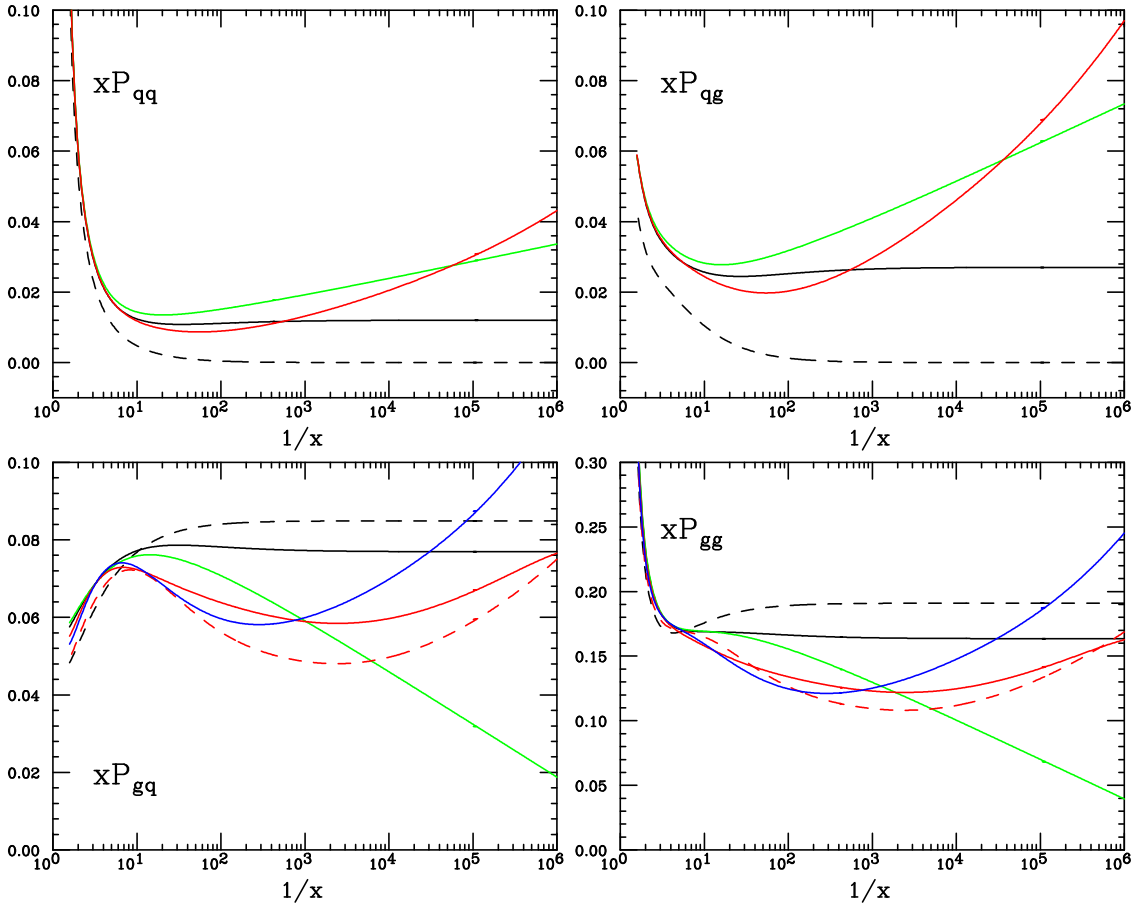

Fig. 4: The resummed splittings functions P_{qq}, P_{qg}, P_{gq} and P_{gg} in the ABF approach, all for $n_f = 4$ and $\alpha_s = 0.2$: LO DGLAP (dashed black), NLO DGLAP (solid black), NNLO DGLAP (solid green), LO resummed (red dashed), NLO resummed in the $\mathrm{Q_0\overline{MS}}$ scheme (red) and in the $\overline{\mathrm{MS}}$ scheme (blue).

$\gamma^B_{ss}(\alpha_{\rm s}(t), N)$ $\gamma^B_{ss,0}(\alpha_{\rm s}(t), N)$ are double counting subtractions between the previous two contributions; $\gamma_{\rm mom}$ subtracts subleading terms which spoil exact momentum conservation; $\gamma_{\rm match}$ subtracts any contribution which deviates from NLO DGLAP and at large N doesn't drop at least as $\frac{1}{N}$.

The anomalous dimension obtained through this procedure has a simple pole as a leading small-N (i.e. small x) singularity, like the LO DGLAP anomalous dimension. The location of the pole is to the right of the DGLAP pole, and it depends on the value of α_s. Thanks to the softening due to running of the coupling, this value is however rather smaller than that which corresponds to the leading BFKL singularity: for example, for $\alpha_s = 0.2$, when $n_f = 0$ the pole is at $N = 0.17$.

The splitting function obtained by Mellin inversion of the anomalous dimension eq. (11)

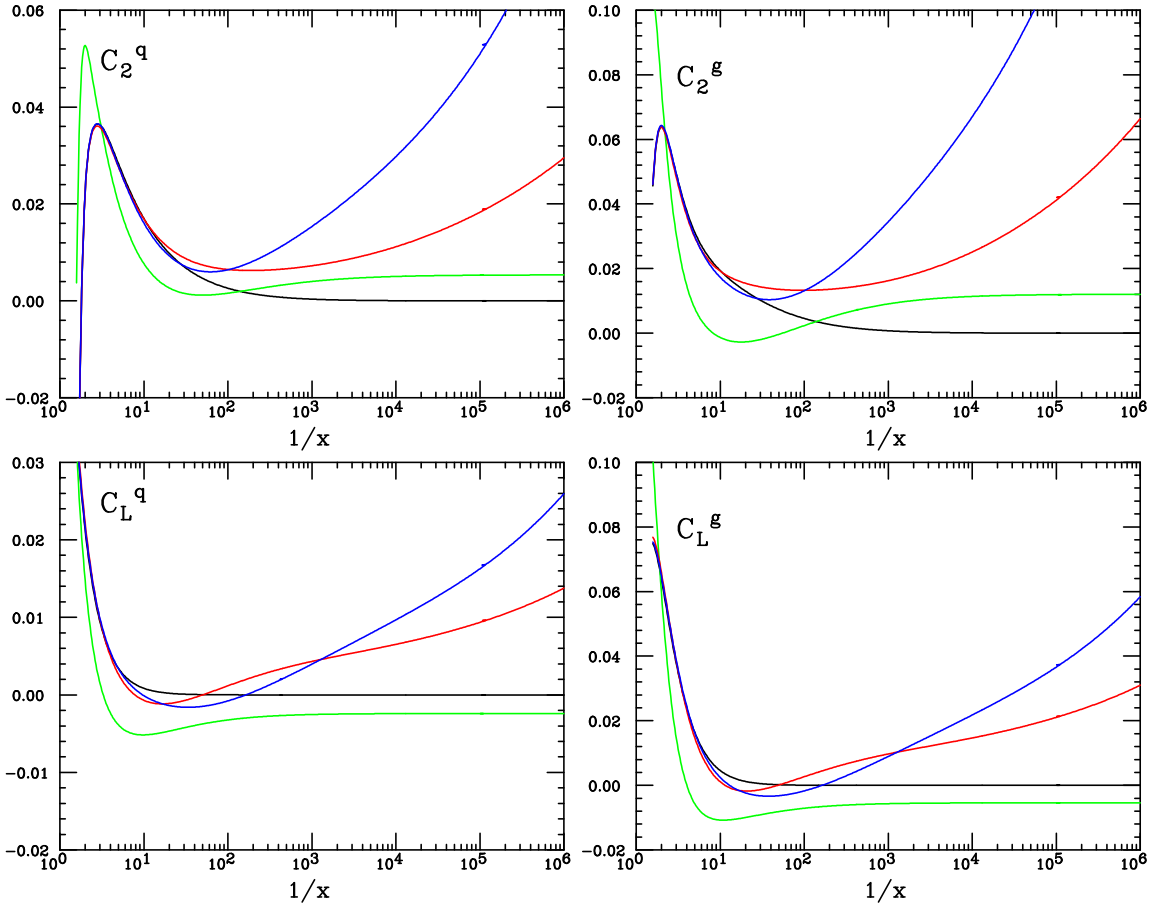

Fig. 5: The resummed DIS coefficient functions C_{2q}, C_{2g}, C_{Lq} and C_{Lg} in the ABF approach, all for $n_f = 4$ and $\alpha_s = 0.2$. The curves are labelled as in the previous figure.

turns out to agree at the percent level to that obtained by the CCSS group by numerical resolution of the BFKL equation for all $x \lesssim 10^{-2}$; for larger values of x (i.e. in the matching region) the ABF result is closer to the NLO DGLAP result.

In order to obtain a full resummation of physical observables, specifically for deep-inelastic scattering, the resummation discussed so far has to be extended to the quark sector and to hard partonic coefficients. This, on top of various technical complications, requires two main conceptual steps:

- A factorization scheme must be defined at a resummed level. Because only one of the two eigenvectors of the matrix of anomalous dimensions is affected by resummation, once a scheme is chosen, the resummation discussed above determines entirely the two-by-two matrix of splitting functions in the singlet sector. The only important requirement is that the relation of this small x scheme choice to standard large x schemes be known exactly,

since this enables one to combine resummed results with known fixed order results.

- PDFs evolved using resummed evolution equations must be combined with resummed coefficient functions. These are known, specifically for DIS [49], but are also known [80] to be affected by singularities, analogous to the running coupling singularities of the resummed anomalous dimension discussed above, which likewise must be resummed to all orders [57]. This running coupling resummation of the coefficient function significantly softens the small x growth of the coefficient function and substantially reduces its scheme dependence [58].

These steps have been accomplished in Ref. [58], where resummed anomalous dimensions (see fig. 4), coefficient functions (see fig.5) and structure functions (see section 2.4 below) have been determined. The scheme dependence of these results can be studied in detail: results have been produced and compared in both the $\overline{\rm MS}$ and $\rm Q_0\overline{MS}$ schemes, and furthermore the variation of results upon variation of factorization and renormalization scales has been studied.

Calculations of resummation corrections not only of deep inelastic processes, but also of benchmark hadronic processes such as Drell-Yan, vector boson, heavy quark and Higgs production are now possible and should be explored.

2.2 The Ciafaloni-Colferai-Salam-Stasto (CCSS) Approach

The Ciafaloni-Colferai-Salam-Stasto (CCSS) resummation approach proposed in a series a papers [47, 60–66] is based on the few general principles:

- We impose the so-called kinematical constraint [81–83] onto the real gluon emission terms in the BFKL kernel. The effect of this constraint is to cut out the regions of the phase space for which $k_T'^2 \geq k_T^2/z$ where k_T, k_T' are the transverse momenta of the exchanged gluons and z is the fraction of the longitudinal momentum.
- The matching with the DGLAP anomalous dimension is done up to the next-to-leading order.
- We impose the momentum sum rule onto the resummed anomalous dimensions.
- Running coupling is included with the appropriate choice of scale. We take the argument of the running coupling to be the transverse momentum squared of the emitted gluon in the BFKL ladder in the BFKL part. For the part which multiplies the DGLAP terms in the eigenvalue equation we choose the scale to be the maximal between k_T^2 and $k_T'^2$.
- All the calculations are performed directly in momentum space. This in particular enables easy implementation of the running of the coupling with the choice of the arguments as described above.

The implementation at the leading logarithmic level in BFKL and DGLAP (and in the single gluon channel case) works as follows. It is convenient to go to the Mellin space representation where we denote by γ and ω the Mellin variables conjugated to $\ln k_T$ and $\ln 1/x$ respectively. The full evolution kernel can be represented as a series $\mathcal{K} = \sum_n \alpha_s^{n+1} \mathcal{K}_n(\gamma, \omega)$. We take the resummed kernel at the lowest order level to be

$$\mathcal{K}_0(\gamma,\omega) \;=\; \frac{2C_A}{\omega}\,\chi_0^{\omega}(\gamma) \;+\; [\gamma_0^{gg}(\omega) - \frac{2C_A}{\omega}]\chi_c^{\omega}(\gamma)\;. \tag{12}$$

The terms in (12) are the following

$$\chi_0^\omega(\gamma) = 2\psi(1) - \psi(\gamma) - \psi(1-\gamma+\omega) \ ,$$

is the leading logarithmic BFKL kernel eigenvalue with the kinematical constraint imposed. This is reflected by the fact that the singularities in the γ plane at $\gamma = 1$ are shifted by the ω. This ensures the compatibility with the DGLAP collinear poles, in the sense that we have only single poles in γ. The function $\chi_c(\gamma)$ is the collinear part of the kernel

$$\chi_c^\omega(\gamma) = \frac{1}{\gamma} + \frac{1}{1-\gamma+\omega} \ ,$$

which includes only the leading collinear poles at $\gamma = 0$ or 1. All the higher twist poles are neglected for this part of the kernel. This kernel eigenvalue is multiplied by the non-singular (in ω) part of the DGLAP anomalous dimension $\gamma_0^{gg}(\omega) - 2C_A/\omega$ where $\gamma_0^{gg}(\omega)$ is the full anomalous dimension at the leading order. The next-to-leading parts both in BFKL and DGLAP are included in the second term in the expansion, i.e. kernel $\mathcal{K}_1$

$$\mathcal{K}_1(\gamma,\omega) = \frac{(2C_A)^2}{\omega}\tilde{\chi}_1^\omega(\gamma) + \tilde{\gamma}_1^{gg}(\omega)\chi_c^\omega(\omega) \tag{13}$$

where $\tilde{\chi}_1^\omega(\gamma)$ is the NLL in x part of the BFKL kernel eigenvalue with subtractions. These subtractions are necessary to avoid double counting: we need to subtract the double and triple collinear poles in γ which are already included in the resummed expression (12) and which can be easily identified by expanding this expression in powers of ω and using the LO relation $\omega = \bar{\alpha}_s\chi_0(\gamma)$. The term $\tilde{\gamma}_1^{gg}(\omega)$ in Eq. (13) is chosen so that one obtains the correct DGLAP anomalous dimension at a fixed next-to-leading logarithmic level. The formalism described above has been proven to work successfully in the single channel case, that is for evolution of gluons only. The solution was shown to be very stable with respect to the changes of the resummation scheme.

The quarks are included in the CCSS approach by a matrix formalism. The basic assumptions in this construction are:

- Consistency with the collinear matrix factorization of the PDFs in the singlet evolution.
- Requirement that only single pole singularities in both in γ and ω are present in the kernel eigenvalues. This assumption allows for the natural consistency with DGLAP and BFKL respectively. Higher order singularities can be generated at higher orders only through the subleading dependencies on these two variables.
- Ability to compute all the anomalous dimensions which can be directly compared with the DGLAP approach. This can be done by using set of recursive equations which allow to calculate the anomalous dimensions order by order from the kernel eigenvalues.
- Impose the collinear-anticollinear symmetry of the kernel matrix via the similarity transformation.
- Incorporate NLLx BFKL and DGLAP up to NLO (and possibly NNLO).

The direct solutions to the matrix equations are the quark and gluon Green's functions. These are presented in Fig. 6 for the case of the gluon-gluon and quark-gluon part. The resulting

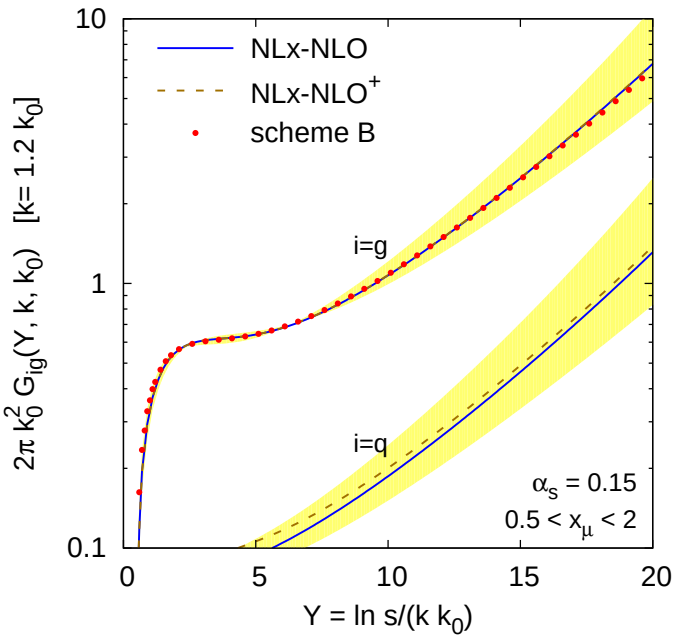

Fig. 6: *Gluon-induced part of the Green function for the NLx-NLO and NLx-NLO$^+$ models, compared to the results the single channel approach. For the models of this paper both gluon-gluon and quark-gluon Green's function are shown. The value chosen for the coupling, $\alpha_s = 0.15$, corresponds to $k_0 \simeq 20\,GeV$. The band indicates the spread in the result for the NLx-NLO model when varying the renormalization scale in the range $0.5 < x_\mu < 2$.*

gluon-gluon part is increasing exponentially with the logarithm of energy $\ln s$ with an effective intercept of about ~ 0.25. It is much suppressed with respect to the leading logarithmic order. We also note that the single channel results and the matrix results for the gluon-gluon Green's function are very similar to each other. In Fig. 6 we also present the quark-gluon channel which is naturally suppressed in normalization with respect to the gluon-gluon one by a factor of the strong coupling constant. This can be intuitively understood as the (singlet) quarks are radiatively generated from the gluons, and therefore this component follows the gluon density very closely. The yellow bands indicate the change of the Green's functions with respect to the change of the scale.

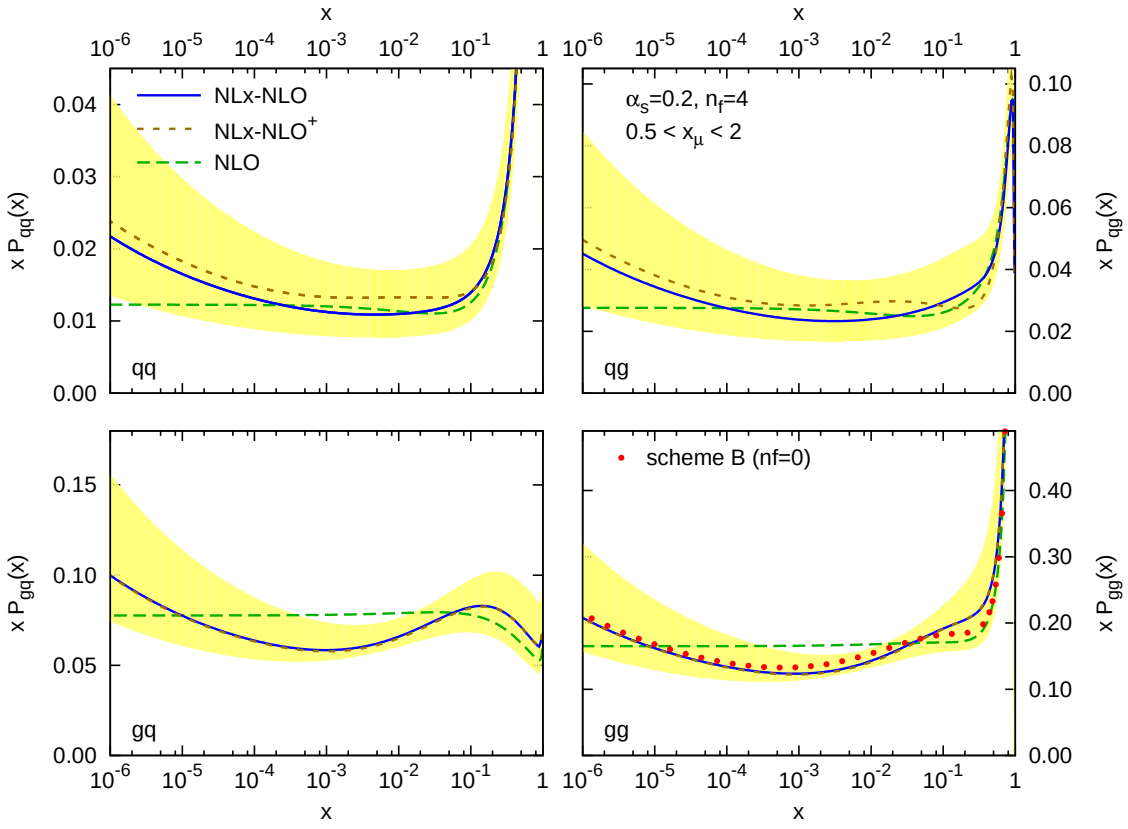

Fig. 7: *The matrix of NLx-NLO (and NLx-NLO$^+$) splitting functions together with their scale uncertainty and the NLO splitting functions for comparison. In the gg channel, we also show the old scheme B result ($n_f = 0$, no NLO contributions, 1-loop coupling) . The band corresponds to the span of results (NLx-NLO) obtained if one chooses $x_\mu = 0.5$ and $x_\mu = 2.0$.*

In Fig. 7 we present all four splitting functions for fixed value of scale Q^2. Here, again the results are very close to the previous single channel approach in the case of the gluon-gluon splitting function. The gluon-quark channel is very close to the gluon-gluon one, with the characteristic dip of this function at about $x \sim 10^{-3}$. The dip delays the onset of rise of the splitting function only to values of x of about 10^{-4}. The scale dependence growths with decreasing x but it is not larger than in the fixed NLO case. The quark-gluon and quark-quark splitting functions

tend to have slightly larger uncertainty due to the scale change but are also slightly closer to the plain NLO calculation. They also tend to have a less pronounced dip structure.

2.3 The Thorne-White (TW) Approach

Substituting the LO running coupling $\bar{\alpha}_S(k^2)$ into equation (5) and performing a double Mellin transform according to equation (6), the BFKL equation 5, as mentioned in Section 2, becomes a differential equation:

$$\frac{d^2 f(\gamma, N)}{d\gamma^2} = \frac{d^2 f_I(\gamma, Q_0^2)}{d\gamma^2} - \frac{1}{\bar{\beta}_0 N}\frac{d(\chi_0(\gamma) f(\gamma, N))}{d\gamma} + \frac{\pi}{3\bar{\beta}_0^2 N}\chi_1(\gamma) f(\gamma, N), \tag{14}$$

where $\chi_{0,1}(\gamma)$ are the Mellin transforms of $\mathcal{K}_{0,1}$. The solution for $f(N, \gamma)$ of Eq. (14) has the following form [61, 84]:

$$f(N, \gamma) = \exp\left(-\frac{X_1(\gamma)}{\bar{\beta}_0 N}\right)\int_\gamma^\infty A(\tilde{\gamma}) \exp\left(\frac{X_1(\tilde{\gamma})}{\bar{\beta}_0 N}\right) d\tilde{\gamma}. \tag{15}$$

Up to power-suppressed corrections, one may shift the lower limit of the integral $\gamma \to 0$, so that the gluon distribution factorises into the product of a perturbative and a non-perturbative piece. The nonperturbative piece depends on the bare input gluon distribution and an in principle calculable hard contribution. However, this latter part is rendered ambiguous by diffusion into the infrared, and in this approach is contaminated by infrared renormalon-type contributions. The perturbative piece is safe from this and is sensitive to diffusion into the ultraviolet region of weaker coupling. Substituting equation (15) into (14), one finds that the perturbative piece is given (after transforming back to momentum space):

$$\mathcal{G}_E^1(N, t) = \frac{1}{2\pi\imath}\int_{1/2-\imath\infty}^{1/2+\imath\infty} \frac{f^{\beta_0}}{\gamma} \exp\left[\gamma t - X_1(\gamma, N)/(\bar{\beta}_0 N)\right] d\gamma, \tag{16}$$

where:

$$X_1(\gamma, N) = \int_{\frac{1}{2}}^{\gamma}\left[\chi_0(\tilde{\gamma}) + N\frac{\chi_1(\tilde{\gamma})}{\chi_0(\tilde{\gamma})}\right] d\tilde{\gamma}. \tag{17}$$

Structure functions F_i also factorize, and the perturbative factors have a similar form to Eq. (16), but involve an additional impact factor $h_i(\gamma, N)$ in the integrand according to the k_t-factorisation theorem [49]. Crucially, coefficient functions and anomalous dimensions involve ratios of the above quantities, such that the non-perturbative factor cancels. Thus, once all the impact factors are known, the complete set of coefficient and splitting functions can be disentangled. Finally they can be combined with the standard NLO DGLAP results (which are known to describe data well at higher x values) using the simple prescription:

$$P^{tot.} = P^{NLL} + P^{NLO} - \left[P^{NLL(0)} + P^{NLL(1)}\right], \tag{18}$$

where P is a splitting or coefficient function, and $P^{NLL(i)}$ the $\mathcal{O}(\alpha_s^i)$ contribution to the resummed result which is subtracted to avoid double-counting. It should be noted that the method

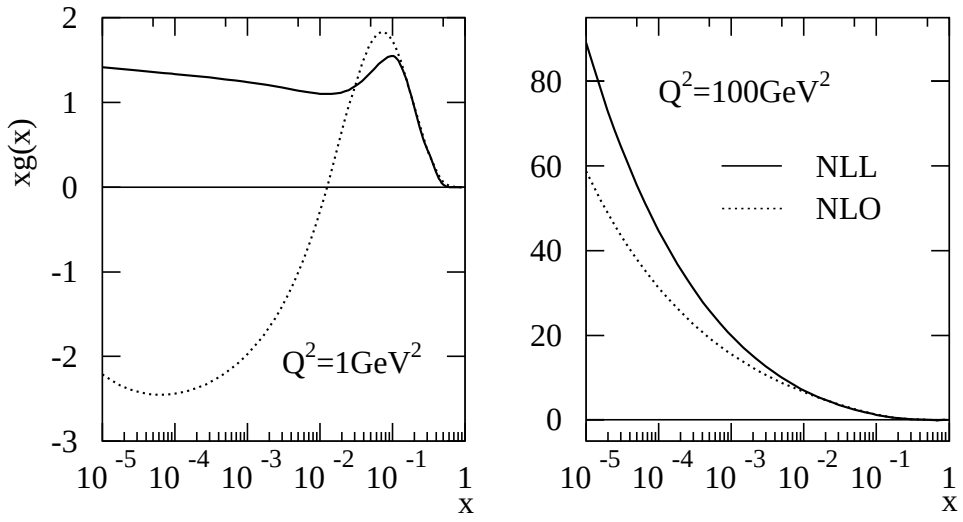

Fig. 8: Gluons arising from a global fit to scattering data including NLL small x resummations in the DIS(χ) factorisation scheme (solid). Also shown is the result from an NLO DGLAP fit in the same scheme.

of subtraction of the resummed contribution in the matching is different to that for the ABF approach outlined after Eq. (11). For example, at NLO in the resummation the BFKL equation provides both the α_S/N part of P_{gg} and the part at $\mathcal{O}(\alpha_S)$ constant as $N \to \infty$. Hence we choose to keep all terms constant as $N \to \infty$ generated by Eq. (16), with similar considerations for other splitting functions and coefficient functions, though these can contain terms $\propto N$. Hence, we include terms which will have some influence out to much higher x than in the ABF approach.

In the TW manner of counting orders LL is defined as the first order at which contributions appear, so while for the gluon splitting function this is for $\bar{\alpha}_S^n \ln^m(1/x)$ for $m = n-1$ for impact factors this is for $m = n-2$. A potential problem therefore arises in that the NLL impact factors are not known exactly. However, the LL impact factors with conservation of energy of the gluon imposed are known in cases of both massless and massive quarks [50, 51], and are known to provide a very good approximation to the full $\mathcal{O}(\alpha_S^2)$ and $\mathcal{O}(\alpha_S^3)$ quark-gluon splitting functions and coefficient functions [85], implying that they must contain much of the important higher-order information. These can then be used to calculate NLL coefficient and splitting functions within a particular factorisation scheme. One must also specify a general mass variable number scheme for consistent implementation of heavy quark mass effects. Such a scheme (called the DIS(χ) scheme) has been given in [71, 72] up to NLL order in the high energy expansion, and

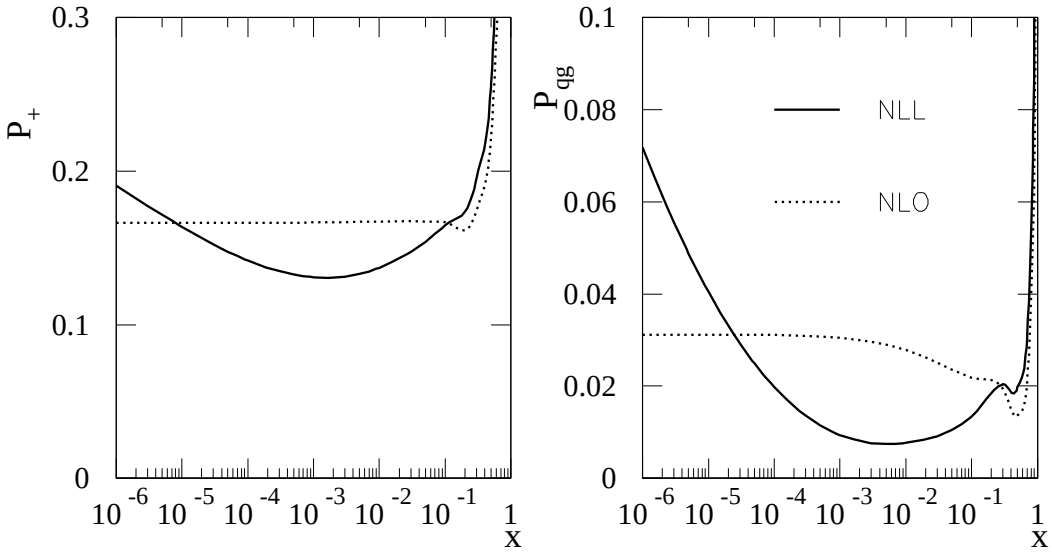

Fig. 9: *The resummed splitting functions (solid)* $P_+ \approx P_{gg}$ *and* P_{qg} *in the TW approach, both for* $n_f = 4$ *and* $\alpha_S = 0.16$*, compared to the corresponding NLO forms (dotted).*

NLO order in the fixed order expansion.

The form of the resummed splitting functions shown in fig. 9 are qualitatively consistent with those from the ABF approach, fig. 4, and CCSS approach fig. 7 (note however that in these plots the value of α_s is a little larger, and the scheme is different). This is despite the fact that the approach does not include the explicit collinear resummation of the BFKL kernel adopted in the other two approaches. It was maintained in [69, 70] that the diffusion into the ultraviolet, effectively making the coupling weaker, hastens the perturbative convergence for splitting functions, and the kernel near $\gamma = 0$, making this additional resummation less necessary. There is no particular obstruction to including this resummation in the approach, it is simply cumbersome. Indeed, in Ref. [70] the effect was checked, and modifications found to be no greater than generic NNLO corrections to the resummation, so it was omitted. (Note that any process where there are two hard scales, sensitive to $\gamma \approx 0.5$, or attempted calculation of the hard input for the gluon distribution, sensitive to $\gamma = 1$, would find this resummation essential.) The main feature of the resummed splitting functions is a significant dip below the NLO DGLAP results, followed by an eventual rise at very low $x \simeq 10^{-5}$. This behaviour drives a qualitative change in the gluon distribution, when implemented in a fit to data.

The combined NLO+NLL splitting and coefficient functions (in the TW approach) have

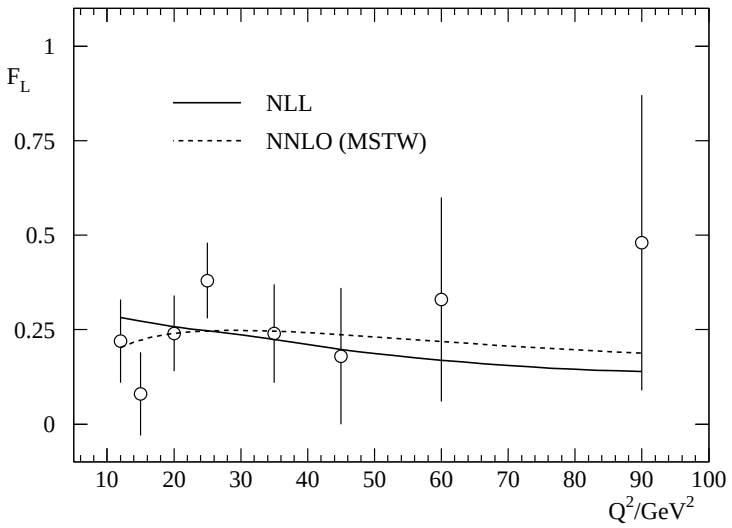

Fig. 10: Recent H1 data on the longitudinal structure function F_L, together with the NLL resummed prediction from the TW approach, and a recent NNLO result from the MSTW group.

been implemented in a global fit to DIS and related data in the DIS(χ) scheme, thus including small x resummations in both the massless and massive quark sectors [72]. The overall fit quality was better than a standard NLO fit in the same factorisation scheme, and a similar NLO fit in the more conventional $\overline{\rm MS}$ factorisation scheme. The principal reason for this is the dip in the resummed evolution kernels, which allows the gluon distribution to increase at both high and low values of x. This reduces a tension that exists between the high x jet data of [86, 87] and the low x HERA data [17, 88–91]. The gluon distributions arising from the NLL and NLO fits are shown in figure 8, for the starting scale $Q^2 = 1{\rm GeV}^2$ and also for a higher value of Q^2. One sees that whilst the NLO gluon wants to be negative at low x and Q^2, the resummed gluon is positive definite and indeed growing slightly as $x \to 0$. The gluons agree well for higher x values (where the DGLAP description is expected to dominate), but deviate for $x \leq 10^{-2}$. This can therefore be thought of as the value of x below which resummation starts to become relevant.

The qualitatively different gluon from the resummed fit (together with the decreased evolution kernels w.r.t. the fixed order description) has a number of phenomenological implications:

1. The longitudinal structure function F_L is sensible at small x and Q^2 values, where the standard DGLAP description shows a marked instability [92].
2. As a result of the predicted growth of F_L at small x the resummed result for the DIS reduced cross-section shows a turnover at high inelasticity y, in agreement with the HERA

data. This behaviour is not correctly predicted by some fixed order fits.

3. The heavy flavour contribution (from charm and bottom) to F_2 is reduced at higher Q^2 in the resummed approach, due mainly to the decreased evolution, as already noted in a full analysis in the fixed-order expansion at NNLO [93]. Nevertheless, it remains a significant fraction of the total structure function at small x.

Other resummation approaches should see similar results when confronted with data, given the qualitative (and indeed quantitative) similarities between the splitting functions. It is the decreased evolution with respect to the DGLAP description that drives the qualitative change in the gluon distribution. This is then the source of any quantitative improvement in the description of data, and also the enhanced description of the longitudinal structure function and reduced cross-section.

The resummed prediction for F_L is shown alongside the recent H1 data [94] in figure 10, and compared with an up-to-date NNLO fixed order result [95]. One sees that the data cannot yet tell apart the predictions, but that they are starting to diverge at low x and Q^2, such that data in this range may indeed be sensitive to the differences between resummed and fixed order approaches.

2.4 Resummed structure functions: comparison of the ABF and TW approaches

In this section, we present an application of the ABF and TW approaches to the resummed determination of the F_2 and F_L deep-inelastic structure functions. The corresponding exercise for the CCSS approach has not yet been finalised. A direct comparison of the two approaches is complicated by issues of factorisation scheme dependence: whereas in the ABF approach results may be obtained in any scheme, and in particular the $\overline{\rm MS}$ and closely related Q_0-$\overline{\rm MS}$ scheme, in the TW formalism splitting functions and coefficient functions beyond NLO in α_S are resummed in the $\rm Q_0$-DIS scheme [65, 96], which coincides with the standard DIS scheme at large x but differs from it at the resummed level; the scheme change needed in order to obtain the coefficient functions from the DIS-scheme ones is performed exactly up to NLO and approximately beyond it. Thus, without a more precise definition of the relation of this scheme to $\overline{\rm MS}$, one cannot compare splitting and coefficient functions, which are factorisation scheme dependent.

A useful compromise is to present the respective results for the ratio of structure function predictions:

$$K_i = \frac{F_i^{NLL}(x,Q^2)}{F_i^{NLO}(x,Q^2)}, \tag{19}$$

where $i \in 2, L$, and the F_i are calculated by convoluting the relevant coefficients with PDFs obtained by perturbative evolution of a common set of of partons, defined at a starting scale of $Q_0^2 = 4\text{GeV}^2$. The number of flavors is fixed to three, to avoid ambiguities due to heavy quark effects. The initial PDFs are assumed to be fixed (i.e., the same at the unresummed and unresummed level) in the DIS factorization scheme at the scale Q_0. Of course, in a realistic situation the data are fixed and the PDFs are determined by a fit to the data: hence they are not the same at the resummed and unresummed level (compare Fig. 8 above). However, in the DIS factorization scheme the structure function F_2 is simply proportional to the quark distribution, hence by fixing the PDFs in this scheme one ensures that F_2 is fixed at the starting scale.

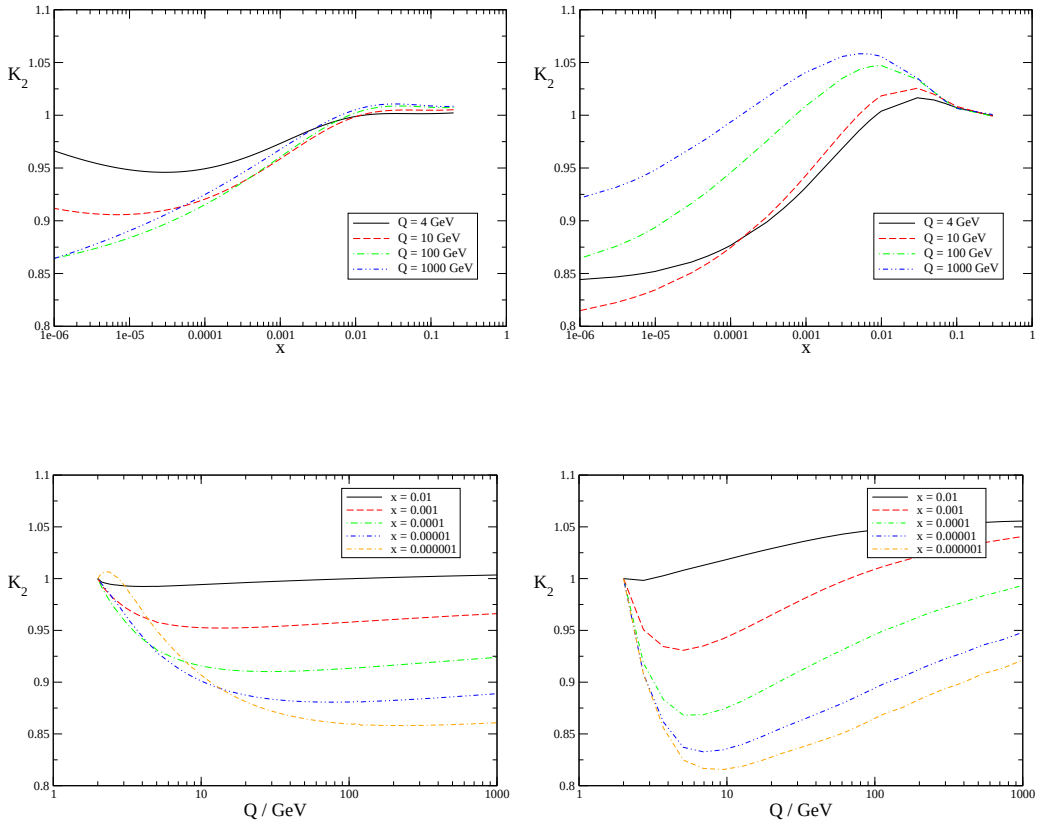

Fig. 11: The ratio F_2^{NLL}/F_2^{NLO} in the ABF approach (left) and the TW approach (right), using toy PDFs, given in eq. 20, calculated as function of x at fixed for Q^2 (upper), and as a function of Q^2 at fixed x (lower).

This starting PDFs are constructed as follows: the quark and gluon distributions are chosen to have the representative form also used in Ref. [58]

$$xg(x) = k_s xS(x) = k_g x^{-0.18}(1-x)^5; \quad xq_v = k_q x^{0.5}(1-x)^4, \tag{20}$$

in the $\overline{\rm MS}$ scheme, where $g(x)$ is the gluon, $S(x)$ the sea quark distribution, and $xq_v(x)$ denotes a valence quark distribution. We choose $k_s = 3$, and then all other parameters are fixed by momentum and number sum rules. Note that the gluon is the same as that used in the previous comparison of Ref. [73]. The PDFs eq. (20) are then transformed to the DIS factorization scheme [97] using the NLO (unresummed) scheme change at the scale Q_0. The result is then used as a fixed boundary condition for all (unresummed and resummed, ABF and TW) calculations. In the TW approach, the DIS scheme for unresummed quantities and $\rm Q_0$DIS scheme as discussed above is then used throughout. In the ABF approach, the fixed DIS-scheme boundary condition is transformed to the $\rm Q_0\overline{MS}$ scheme [58,98] (which at the unresummed level coincides with standard $\overline{\rm MS}$) by using the unresummed or resummed scheme change function as appropriate, and then all calculations are performed in $\rm Q_0\overline{MS}$. One might hope that most of the residual scheme dependence cancels upon taking the ratio of the NLL and NLO results, at least for schemes that

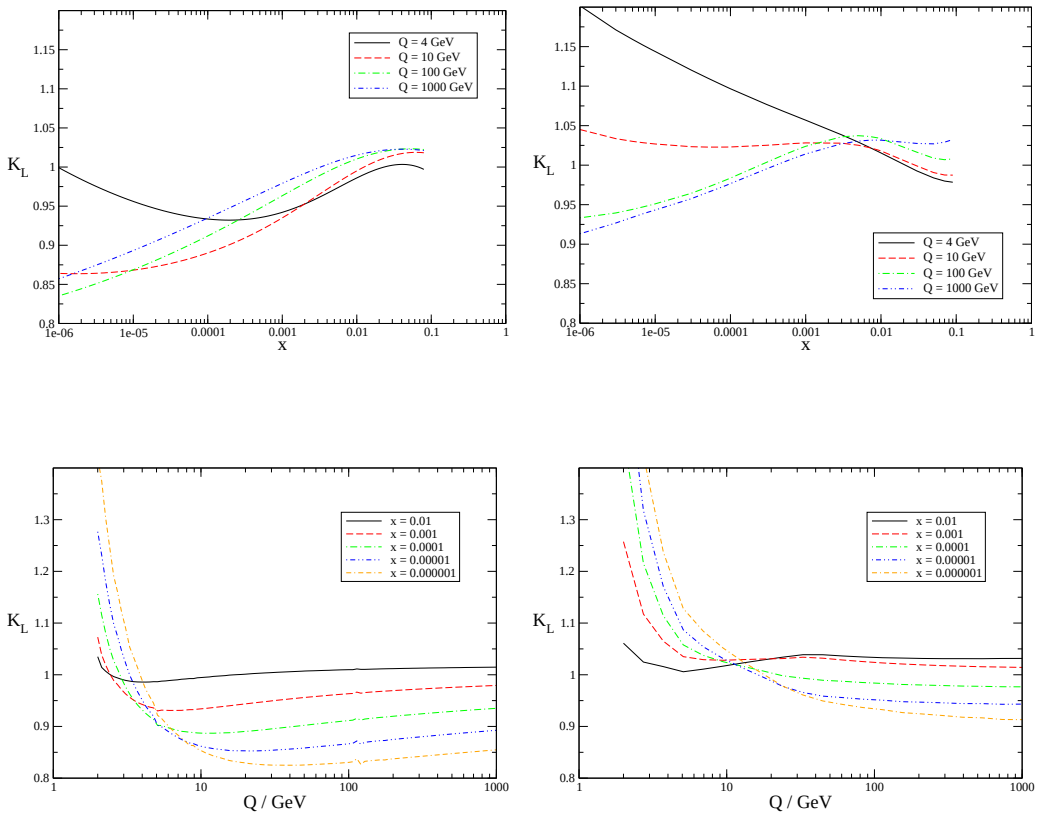

Fig. 12: The ratio F_L^{NLL}/F_L^{NLO} in the ABF approach (left) and the TW approach (right), using toy PDFs, given in eq. 20, calculated as function of x at fixed for Q^2 (upper), and as a function of Q^2 at fixed x (lower).

are well defined and without unphysical singularities.

The results for K_2 and K_L are shown in figures 11 for F_2 in the ABF and TW procedures respectively and similarly in figures 12 for F_L. One sees that for x sufficiently small, and for Q not too large, the resummed F_2 is consistently lower than its fixed order counterpart in both approaches, due to the decreased evolution of the gluon, and also (in the $\overline{\rm MS}$ scheme) due to the fact that resummed coefficient functions are much larger than the NLO ones at small x and low Q^2. Similarly the resummed F_L is larger than the fixed order at low Q and small enough x, but falls rapidly as Q increases. However despite these superficial similarities, the two approaches differ quantitatively in several respects:

- the ABF resummed F_2 matches well to the NLO for $x \gtrsim 10^{-2}$ at all scales, while the TW F_2 shows a rise around $x \simeq 10^{-2}$, which is largest at low Q. This may be due to the significant differences between resummed and NLO splitting functions at very high x in fig. 9. A similar mismatch may be seen at $x \sim 0.1$ in the F_L K-factor.
- at large scales the ABF resummation stabilises, due to the running of the coupling, so the K-factors becomes rather flat: they grow only logarithmically in $\ln Q$. By contrast the TW F_2 K-factor still shows a marked Q^2 dependence. This may be related to the fact that the

TW resummation does not resum the collinear singularities in the BFKL kernel, and to the TW choice (see Sect. 2.3) not to include subtraction of terms induced by the resummation which do not drop at large x. This choice induces a change in the PDFs at higher x in the TW approach, which results in effects which persist to higher Q^2 at smaller x.

- at the initial scale Q_0 the TW resummed F_L grows much more strongly as x decreases than the ABF resummed F_L. This is likely to be due to the different treatment of the coefficient functions: in this respect, the fully consistent treatment of the factorization scheme, the effect of collinear resummation, and the different definitions of what is called resummed NLO used by the two groups all play a part.

2.5 Conclusion

The problem of understanding the small x evolution of structure functions in the domain of x and Q^2 values of relevance for HERA and LHC physics has by now reached a status where all relevant physical ingredients have been identified, even though not all groups have quite reached the stage at which the formalism can be transformed into a practical tool for a direct connection with the data.

In this report we summarised the status of the three independent approaches to this problem by ABF, CCSS and TW, we discussed the differences in the adopted procedures and finally we gave some recent results. The most complete formalisms are those by ABF and CCSS while the TW approach is less comprehensive but simpler to handle, and thus has been used in fit to data. We recall that, at the level of splitting functions the ABF and CCSS have been compared in ref. [73] and found to be in very good agreement. The singlet splitting function obtained by TW was also compared with ABF and CCSS in ref. [72] and also found to be in reasonable agreement, at least at small x.

Here we have shown the results of an application to the structure functions F_2 and F_L of the ABF and TW methods. The same input parton densities at the starting scale Q_0 were adopted by these two groups and the K-factors for resummed versus fixed NLO perturbative structure functions were calculated using the respective methods. The results obtained are in reasonable qualitative agreement for F_2, less so for F_L. Discrepancies may in part be due to the choice of factorization scheme, but our study suggests that the following are also likely to make a quantitative difference: whether or not a resummation of collinear singularities in the BFKL kernel is performed, whether contributions from the resummation which persist at large x are subtracted and whether the factorization scheme is consistently defined in the same way at resummed and NLO levels.

3 Parton saturation and geometric scaling[3]

3.1 Introduction[4]

The degrees of freedom involved in hadronic collisions at sufficiently high energy are partons, whose density grows as the energy increases (i.e., when x, their momentum fraction, decreases). This growth of the number of gluons in the hadronic wave functions is a phenomenon which has

[3]Contributing authors: G. Beuf, F. Caola, F. Gelis, L. Motyka, C. Royon, D. Šálek, A. M. Stašto

[4]Contributing authors: F. Gelis, A. M. Stašto

been well established at HERA. One expects however that it should eventually "saturate" when non linear QCD effects start to play a role.

An important feature of partonic interactions is that they involve only partons with comparable rapidities. Consider the interaction between a hadron and some external probe (e.g. a virtual photon in Deep Inelastic Scattering) and consider what happens when one boosts the hadron, increasing its rapidity in successive steps. In the first step, the valence constituents become Lorentz contracted in the longitudinal direction while the time scale of their internal motions is Lorentz dilated. In addition, the boost reveals new vacuum fluctuations coupled to the boosted valence partons. Such fluctuations are not Lorentz contracted in the longitudinal direction, and represent the dynamical degrees of freedom; they are the partons that can interact with the probe. Making an additional step in rapidity would freeze these fluctuations, while making them Lorentz contracted as well. But the additional boost also produces new quantum fluctuations, which become the new dynamical variables. This argument can be repeated, and one arrives at the picture of a high-energy projectile containing a large number of frozen, Lorentz contracted partons (the valence partons, plus all the quantum fluctuations produced in the previous boosts), and partons which have a small rapidity, are not Lorentz contracted and can interact with the probe. This space-time description was developed before the advent of QCD (see for instance [99]; in Bjorken's lectures [100], one can actually foresee the modern interpretation of parton evolution as a renormalization group evolution).

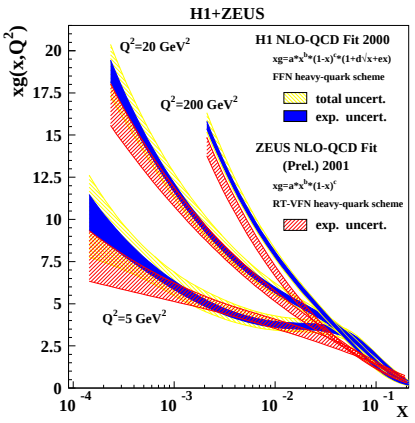

Fig. 13: The gluon structure function in a proton measured at HERA.

This space-time picture, which was deduced from rather general considerations, can now be understood in terms of QCD. In fact, shortly after QCD was established as the theory of strong interaction, quantitative equations were established, describing the phenomenon outlined above [41, 101–105]. In particular, the equation derived by Balitsky, Fadin, Kuraev and Lipatov [41, 101] describes the growth of the non-integrated gluon distribution in a hadron as it is boosted towards higher rapidities. Experimentally, an important increase of the number of gluons at small x has indeed been observed in the DIS experiments performed at HERA (see Fig. 13), down to $x \sim 10^{-4}$. Such a growth raises a problem: if it were to continue to arbitrarily small x, it would induce an increase of hadronic cross-sections as a power of the center of mass energy, in violation of known unitarity bounds.

However, as noticed by Gribov, Levin and Ryskin in [106], the BFKL equation includes only branching processes that increase the number of gluons ($g \to gg$ for instance), but not the recombination processes that could reduce the number of gluons (like $gg \to g$). While it may be legitimate to neglect the recombination process when the gluon density is small, this cannot remain so at arbitrarily high density: a saturation mechanism of some kind must set in. Treating the partons as ordinary particles, one can get a crude estimate

of the onset of saturation, which occurs at:

$$Q^2 = Q_s^2 \ , \quad \text{with } Q_s^2 \sim \alpha_s(Q_s^2)\frac{xG(x,Q_s^2)}{\pi R^2} \ . \tag{21}$$

The momentum scale that characterizes this new regime, Q_s, is called the saturation momentum [107]. Partons with transverse momentum $Q > Q_s$ are in a dilute regime; those with $Q < Q_s$ are in the saturated regime. The saturation momentum increases as the gluon density increases. This comes from an increase of the gluon structure function as x decreases. The increase of the density may also come from the coherent contributions of several nucleons in a nucleus. In large nuclei, one expects $Q_s^2 \propto A^{1/3}$, where A is the number of nucleons in the nucleus.

Note that at saturation, naive perturbation theory breaks down, even though $\alpha_s(Q_s)$ may be small if Q_s is large: the saturation regime is a regime of weak coupling, but large density. At saturation, the gluon occupation number is proportional to $1/\alpha_s$. In such conditions of large numbers of quanta, classical field approximations become relevant to describe the nuclear wave-functions.

Once one enters the saturated regime, the evolution of the parton distributions can no longer be described by a linear equation such as the BFKL equation. The color glass condensate formalism (for a review, see [108]), which relies on the separation of the degrees of freedom in a high-energy hadron into frozen partons and dynamical fields, as discussed above, provides the non linear equations that allow us to follow the evolution of the partonic systems form the dilute regime to the dense, saturated, regime. For instance, the correlator $\mathrm{tr}\langle U^\dagger(\boldsymbol{x}_\perp)U(\boldsymbol{y}_\perp)\rangle$ of two Wilson lines –which enters in the discussion of DIS– evolves according to the Balitsky-Kovchegov [109, 110] equation:

$$\frac{\partial \mathrm{tr}\langle U^\dagger(\boldsymbol{x}_\perp)U(\boldsymbol{y}_\perp)\rangle_x}{\partial \ln(1/x)} = -\frac{\alpha_s}{2\pi^2}\int_{\boldsymbol{z}_\perp} \frac{(\boldsymbol{x}_\perp-\boldsymbol{y}_\perp)^2}{(\boldsymbol{x}_\perp-\boldsymbol{z}_\perp)^2(\boldsymbol{y}_\perp-\boldsymbol{z}_\perp)^2}$$
$$\times\Big[N_c \mathrm{tr}\langle U^\dagger(\boldsymbol{x}_\perp)U(\boldsymbol{y}_\perp)\rangle_x - \mathrm{tr}\langle U^\dagger(\boldsymbol{x}_\perp)U(\boldsymbol{z}_\perp)\rangle_x \mathrm{tr}\langle U^\dagger(\boldsymbol{z}_\perp)U(\boldsymbol{y}_\perp)\rangle_x\Big] \ . \tag{22}$$

(This equation reduces to the BFKL equation in the low density limit.)

The geometric scaling phenomenon was first introduced in the context of the dipole picture of the deep inelastic electron-proton scattering [111]. The process of the scattering of the virtual photon on a proton at very small values of x can be conveniently formulated in the dipole model. In this picture the photon fluctuates into the quark-antiquark pair (dipole) and subsequently interacts with the target. In the small x regimes these two processes factorize and they can be encoded into the dipole formula for the total $\gamma^* p$ cross section

$$\sigma_{T,L}(x,Q^2) \ = \ \int d^2\mathbf{r}\int dz |\Psi_{T,L}(r,z,Q^2)|^2 \, \hat{\sigma}(x,r) \tag{23}$$

where $\Psi_{T,L}$ is the wave function for the photon and $\hat{\sigma}$ is the dipole cross section. r is the dipole size and z is the light-cone fraction of the longitudinal momentum carried by the quark (or antiquark). The photon wave functions Ψ are known, the dipole cross section can be expressed in terms of the correlator of Wilson lines whose evolution is driven by Eq. (22) :

$$\hat{\sigma}(x,r) = \frac{2}{N_c}\int d^2\boldsymbol{X} \ \mathrm{tr}\Big\langle 1 - U(\boldsymbol{X}+\frac{\mathbf{r}}{2})U^\dagger(\boldsymbol{X}-\frac{\mathbf{r}}{2})\Big\rangle \ . \tag{24}$$

Alternatively, it can be modeled or extracted from the data. In the GBW model it was assumed that the dipole cross section has a form

$$\hat{\sigma} = \sigma_0 \left[1 - \exp(-r^2/R_0(x)^2)\right] \tag{25}$$

where $R_0(x) = (x/x_0)^{-\lambda}$ is a saturation radius (its inverse is usually called the saturation scale $Q_s(x)$) and σ_0 a normalisation constant. One of the key properties of the model was the dependence on the dipole size and the Bjorken x through only one combined variable $r^2 Q_s^2(x)$. This fact, combined with the property of the dipole formula, allows to reformulate the total cross section as a function of $Q^2/Q_s^2(x)$ only. This feature is known as the geometric scaling of the total $\gamma^* p$ cross section. Initially postulated as a property of the GBW model, it was then shown that the experimental data do indeed exhibit the aforementioned regularity in a rather wide range of Q^2 and for small values of Bjorken x.

Although it is a postulate in the GBW model, this property can be derived from the small-x behavior of the solutions of Eq. (22) [112] : for a wide class of initial conditions, the BK equation drives its solution towards a function that obeys this scaling. Note also that the saturation scale, introduced by hand in the GBW model, is dynamically generated by the non linear evolution described by Eq. (22). This suggested that the regularity seen in the data could be explained by the scaling property of the solutions to the nonlinear equations in the saturated regime - and thus may provide some indirect evidence for gluon saturation.

Nevertheless, several important questions remained. One of them, is the problem of the compatibility of the DGLAP evolution with the property of the geometric scaling. It is known from the global fits that the standard DGLAP evolution works quite well for the description of the of the deep inelastic data even in the very low x and Q^2 regime. That suggests that the saturation should be confined to the very tight kinematic regime, and it is therefore questionable whether the observed regularity could be attributed to the saturation at all. In the present contribution we discuss several approaches to this problem.

3.2 Phenomenology[5]

In order to compare the quality of different scaling laws, it is useful to use a quantity called *quality factor* (QF). It is also used to find the best parameters for a given scaling. In the following, this method is used to compare the scaling results for the proton structure function F_2 and F_2^c, the deeply virtual Compton scattering, the diffractive structure function, and the vector meson cross section data measured at HERA.

Quality Factor Given a set of data points $(Q^2, x, \sigma = \sigma(Q^2, x))$ and a parametric scaling variable $\tau = \tau(Q^2, Y, \lambda)$ (with $Y = \ln 1/x$) we want to know whether the cross-section can be parametrised as a function of the variable τ only. Since the function of τ that describes the data is not known, the QF has to be defined independently of the form of that function.

For a set of points (u_i, v_i), where u_i's are ordered and normalised between 0 and 1, we

[5]Contributing authors: C. Royon, D. Šálek

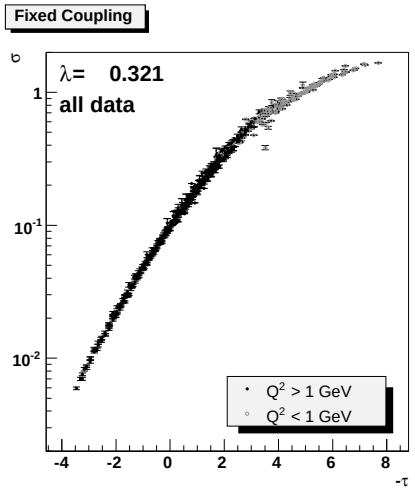

Fig. 14: F_2 **data:** Scaling curve $\sigma = \sigma(\tau)$ for "Fixed Coupling". A $Q^2 > 1$ GeV^2 cut was applied to the data.

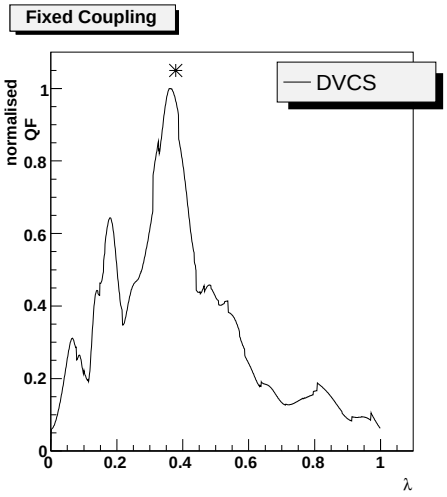

Fig. 15: **DVCS data:** Quality factor normalised to 1 plotted against the parameter λ. Star denotes the fit result for F_2 data.

introduce QF as follows [113]

$$QF(\lambda) = \left[\sum_i \frac{(v_i - v_{i-1})^2}{(u_i - u_{i-1})^2 + \epsilon^2}\right]^{-1}, \tag{26}$$

where ϵ is a small constant that prevents the sum from being infinite in case of two points have the same value of u. According to this definition, the contribution to the sum in (26) is large when two successive points are close in u and far in v. Therefore, a set of points lying close to a unique curve is expected to have larger QF (smaller sum in (26)) compared to a situation where the points are more scattered.

Since the cross-section in data differs by orders of magnitude and τ is more or less linear in $log(Q^2)$, we decided to take $u_i = \tau_i(\lambda)$ and $v_i = log(\sigma_i)$. This ensures that low Q^2 data points contribute to the QF with a similar weight as higher Q^2 data points.

Fits to F_2 and DVCS Data We choose to consider all available data from H1, ZEUS, NMC and E665 experiments [17, 89–91, 114–117] with Q^2 in the range $[1; 150]$ GeV^2 and $x < 0.01$[6]. We exclude the data with $x > 10^{-2}$ since they are dominated by the valence quark densities, and the formalism of saturation does not apply in this kinematical region. In the same way, the upper Q^2 cut is introduced while the lower Q^2 cut ensures that we stay away from the soft QCD domain. We will show in the following that the data points with $Q^2 < 1$ GeV^2 spoil the fit stability. Two kinds of fits to the scaling laws are performed, either in the full mentioned Q^2 range, or in a tighter Q^2 range $[3; 150]$ GeV^2 to ensure that we are in the domain where perturbative QCD applies.

[6]The data in the last ZEUS paper include contributions for F_L and xF_3 but those can be neglected within the kinematical domain we consider.

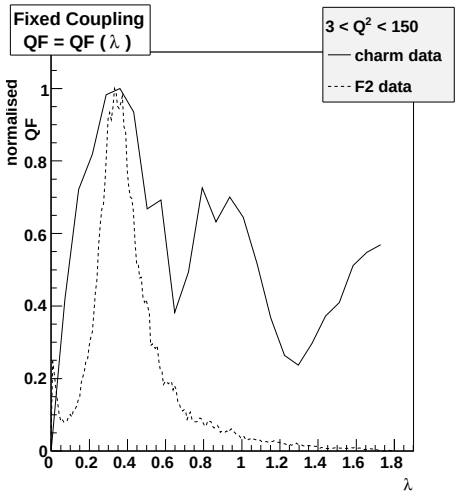

Fig. 16: F_2^c **data:** Comparison of the λ parameter for F_2 and F_2^c data for $Q^2 > 3$ GeV^2.

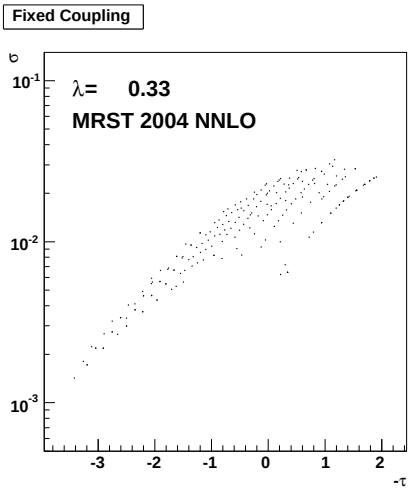

Fig. 17: F_2^c **parametrisation:** Scaling curve $\sigma = \sigma(\tau)$ for fixed coupling using the MRST 2004 NNLO parametrisation for $\lambda = 0.33$ as obtained in the fit to experimental data. No scaling is observed for $Q^2 > 3$ GeV^2.

Figure 14 shows the scaling plot for "Fixed Coupling" in the Q^2 range $[1; 150]$ GeV^2, which shows that the lowest Q^2 points in grey have a tendency to lead to worse scaling. The QF values are similar for the "Fixed Coupling", "Running Coupling I", and "Running Coupling IIbis" — with a tendency to be slightly better for "Running Coupling IIbis" — and worse for diffusive scaling [118].

The amount of the DVCS data [119, 120] measured by H1 and ZEUS is smaller (34 points for H1 and ZEUS requiring $x \leq 0.01$ as for F_2 data), therefore the precision on the λ parameter is weaker. The kinematic coverage of the DVCS data covers smaller region in x and Q^2 than F_2: $4 < Q^2 < 25$ GeV^2 and $5 \cdot 10^{-4} < x < 5 \cdot 10^{-3}$. The DVCS data lead to similar λ values as in the F_2 data (see Fig. 15), showing the consistency of the scalings. The values of the QF show a tendency to favour "Fixed Coupling", but all different scalings (even "Diffusive Scaling") lead to reasonable values of QF.

Implications for Diffraction and Vector Mesons We used the values of the parameters obtained from the fit to F_2 data to test the various scaling variables on the diffractive cross section and vector meson data [121–123]. We tested both the fixed β scaling behaviour in $x_{I\!P}$ and the fixed $x_{I\!P}$ scaling behaviour in β. At fixed β, we find a scaling behaviour up to $\beta = 0.65$. At fixed $x_{I\!P}$, the scaling behaviour of the diffractive cross section as a function of β and Q^2 is far less obvious. This is not a surprise, as not enough data is available in the genuine small β region. A sign of scaling is however observed for the $x_{I\!P} = 0.03$ bin.

Concerning ρ, J/Ψ, and ϕ production [124–126], we found a reasonable scaling behaviour for all tested scaling variables, with the hard scale $Q^2 + M_V^2$, borrowed from vector mesons

wave function studies. Surprisingly, the best scaling is for all three vector mesons the "Diffusive scaling".

Fits to F_2 and F_2^c in QCD Parametrisations First we test the scaling properties using experimental F_2^c data. The requirements on the kinematical domain remain the same as in the case of F_2 studies. The lower $Q^2 > 3$ GeV^2 cut also allows to remove eventual charm mass effects. We use the charm F_2^c measurements from the H1 and ZEUS experiments [127–130]. Only 25 data points lie in the desired kinematical region.

Since the statistics in the data is low, the fit results are not precise. Nevertheless, they still lead to clear results that are comparable to F_2 fits. The results are found similar between F_2 and F_2^c (see Fig. 16). All λ parameters are similar for F_2 and F_2^c except for "Diffusive Scaling". As in the case of the F_2 scaling analysis, "Fixed Coupling", "Running Coupling I" and "Running Coupling II" give similar values of QF, and "Diffusive Scaling" is disfavoured.

The QCD parametrisations [131–133] of the structure function have been tested using CTEQ, MRST, GRV. The same Q^2 and x points as in the experimental data were taken into account. Parametrisations of F_2 are able to reproduce the scaling results seen in the experimental data. However, they are not successful in describing the scaling properties in case of F_2^c. Fig. 17 shows the scaling curve of "Fixed Coupling" in the MRST NNLO 2004 parametrisation of F_2^c where the value of $\lambda = 0.33$ is imposed (as seen in the experimental data). The scaling curve is plotted with all the points used in the F_2 study. Therefore the fact that there is not just a single scaling curve in F_2^c parametrisation is not in direct disagreement with the data — with 25 point only, the curves in parametrisation and data look similar. However the fit values of λ are different.

The CTEQ, MRST or GRV parametrisations are unable to reproduce the scaling properties in F_2^c. It seems a sea-like intrinsic charm component like the one used in CTEQ 6.6 C4 helps to get results closer to a single scaling curve [134]. Scaling is not present at all in the MRST or GRV parametrisations at low Q^2.

3.3 Geometric scaling and evolution equations with saturation[7]

Let us now recall how scaling properties arise from saturation, as shown in [112], using methods and results from non-linear physics (see [135, 136] for alternative demonstrations). Our discussion, independent of the precise saturation formalism, is valid *e.g.* for the JIMWLK and BK equations (see [108] and references therein), at LL, NLL or even higher order in $\log(1/x)$. We will discuss separately the fixed and the running α_s cases, as running coupling is the main effect which can modify the discussion.

Saturation amounts to add a non-linear damping contribution to the BFKL evolution. One writes formally the evolution equation at LL for the dipole-proton cross section $\hat{\sigma}$ (23)

$$\partial_Y \hat{\sigma}(Y, L) = \bar{\alpha}\chi(-\partial_L)\hat{\sigma}(Y, L) - \text{non-linear terms in } \hat{\sigma}(Y, L) \,, \tag{27}$$

where $Y \equiv \log(1/x)$, $L \equiv -\log(r^2\Lambda_{QCD}^2)$ and $\chi(\gamma)$ is the characteristic function of the BFKL kernel. The nonlinear damping ensures that, for any Y, $\hat{\sigma}(Y, L)$ grows at most as a power of

[7] Contributing author: G. Beuf

$|L|$ for $L \to -\infty$ (*i.e.* $r \to +\infty$). The color transparency property of the dipole cross section implies $\hat{\sigma}(Y, L) \propto e^{-L}$ for $L \to +\infty$. Using a double Laplace transform with partial waves $e^{-\gamma L + \omega Y}$, the linear part of (27) reduces to the BFKL dispersion relation $\omega = \bar{\alpha}\chi(\gamma)$, which gives the partial waves solutions $e^{-\gamma[L - \bar{\alpha}\chi(\gamma)Y/\gamma]}$. In the relevant interval $0 < \gamma < 1$, the phase velocity $\lambda(\gamma) = \bar{\alpha}\chi(\gamma)/\gamma$ has one minimum, for the critical value $\gamma = \gamma_c \simeq 0.63$ which is the solution of $\chi(\gamma_c) = \gamma_c \chi'(\gamma_c)$. In the presence of saturation terms in the evolution equation, the wave with $\gamma = \gamma_c$ is selected dynamically.

In order to understand the dynamics of the problem, let us consider an arbitrary initial condition, at some rapidity $Y = Y_0$. With the definition $\gamma_{eff}(L, Y) \equiv -\partial_L \log(\hat{\sigma}(Y, L))$, $\gamma_{eff}(L, Y_0)$ gives the exponential slope of the initial condition in the vicinity of L. That vicinity will then propagates for $Y \geq Y_0$ at a velocity $\lambda(\gamma_{eff}(L, Y)) = \bar{\alpha}\chi(\gamma_{eff}(L, Y))/\gamma_{eff}(L, Y)$. One finds easily that, if $\gamma_{eff}(L, Y_0)$ is a growing function of L, the regions of smaller velocity will spread during the Y evolution, and invade the regions of larger velocity. Restricting ourselves to initial conditions verifying the saturation at $L \to -\infty$ and the color transparency at $L \to +\infty$ as discussed previously, one obtains that $\gamma_{eff}(L, Y_0)$ goes from 0 at low L to 1 at large L. At intermediate L, $\gamma_{eff}(L, Y_0)$ will cross the value γ_c, corresponding to the minimal velocity $\lambda_c = \lambda(\gamma_c)$. Hence, one conclude that, as Y grows, there is a larger and larger domain in L where $\gamma_{eff}(L, Y) = \gamma_c$ and thus $\lambda = \lambda_c$. In that domain, one has $\hat{\sigma}(Y, L) \propto e^{-\gamma_c(L - \lambda_c Y)}$, and hence the geometric scaling $\hat{\sigma}(Y, L) \equiv f(L - \lambda_c Y) = f(-\log(r^2 Q_s^2(x)))$, with a saturation scale $Q_s^2(x) = e^{\lambda_c Y}\Lambda_{QCD}^2 = x^{-\lambda_c}\Lambda_{QCD}^2$. One finds that the geometric scaling window is limited to $L < \lambda_c Y + \sqrt{\bar{\alpha}\chi''(\gamma_c)Y/2}$, and separated from the region still influenced by the initial condition by a cross-over driven by BFKL diffusion. So far, we discussed only scaling properties of the dipole cross section $\hat{\sigma}$. As explained in the introduction, they imply similar scaling properties of the virtual photon-proton cross section, with the replacement $r \mapsto 1/Q$.

The mechanism of wave selection explained above happens mainly in the linear regime[8], *i.e.* for small $\hat{\sigma}$, or equivalently r smaller than $Q_s^2(x)$. However, the geometric scaling property stays also valid in the non-linear regime, *i.e.* for r larger than $Q_s^2(x)$, which is reached after a large enough evolution in Y. The only, but decisive, role of saturation in the linear domain is to provide the following dynamical boundary condition in the IR to the linear BFKL evolution: when $\hat{\sigma}$ is large, it should be quite flat ($\gamma_{eff}(L) \simeq 0$). Indeed, one can simulate successfully the impact of saturation on the solution in the linear regime by studying the BFKL evolution in the presence of an absorptive wall [136], set at a Y-dependent and selfconsistently determined position near the saturation scale.

At NLL and higher order level, the terms different from running coupling ones do not affect the previous discussion. They just change the kernel eigenvalues $\chi(\gamma)$ and thus shift the selected parameters γ_c and λ_c. On the contrary, going from fixed to running coupling brings important changes. As the mechanism of spreading of smaller velocity regions of the solution towards larger velocity ones is local, one expect that it holds in the running coupling case. But it selects coupling-dependent velocity and shape of the front, the coupling itself being L-dependent. Hence, the picture is the following. We still have the formation of a specific traveling wave front solution, which progressively loses memory of its initial condition. However, the selected values

[8] We call linear (non-linear) regime the (Y,L) domain where the explicit value of the non-linear terms in (27) is (is not) negligible compared to the value of the linear terms.

of the velocity and shape of the front drift as the front propagate towards larger L (smaller r), due to asymptotic freedom. So far, this running coupling case has been solved analytically [112, 136] only at large L and large Y, keeping the relevant geometric scaling variable $-\log(r^2 Q_s^2(x))$ finite. One finds that the evolution is slower than in the fixed coupling case, as the large Y behavior of the saturation scale is now $Q_s^2(x) \sim e^{\sqrt{v_c Y/b}} \Lambda_{QCD}^2$, with $b \equiv (33 - 2N_f)/36$ and $v_c \equiv 2\chi(\gamma_c)/\gamma_c$. In addition, the geometric scaling window is narrower: asymptotically in Y, it is expected to hold only for[9] $L < \sqrt{v_c Y/b} + (|\xi_1|/4)\ (\chi''(\gamma_c))^{1/3} Y^{1/6}/(2b\gamma_c\chi(\gamma_c))^{1/6}$. The convergence of the selected front towards this asymptotic solution seems rather slow, which may weaken its phenomenological relevance. The whole theoretical picture is nevertheless consistent with numerical simulations [137, 138]. Both leads to a universal traveling wave front structure of the solution, implying scaling properties also subasymptotically.

In order to do phenomenological studies, one can try to extrapolate to finite L and Y the scaling behavior found asymptotically. However, this extrapolation is not unique [139]. There is indeed an infinite family of scaling variables

$$\tau_\delta \equiv \left[1 - \left(\frac{v_c Y}{bL^2}\right)^\delta\right] L, \tag{28}$$

parameterized by δ, which are different from each other at finite L and Y but all converge to the same asymptotic scaling previously mentioned. The parameter δ seems quite unconstrained, both from the theory and from the DIS data, as shown in the phenomenological section of the present contribution. We considered as benchmark points in that family two specific choices of δ. The choice $\delta = 1/2$ leads to the only scaling variable of the family which is a genuine geometric scaling variable, *i.e.* is equivalent to a scaling with $r^2 Q_s^2(x)$. It is named *running coupling I* in the phenomenological section. The choice $\delta = 1$ leads to the scaling variable obtained by substitution of the fixed coupling by the running coupling directly in the original fixed coupling geometric scaling variable. It is called *running coupling II*.

Finally, one expects scaling properties in any case from evolution equations with saturation, both in the non-linear regime, and in a scaling window in the linear regime. In the linear regime, the solution still obey the linearized equation, and saturation play only the role of a dynamically generated boundary condition. Hence, geometric scaling there, although generated by saturation, is not a hint against the validity of PDF fits. However, geometric scaling occurs also in the non-linear regime, where the scaling function is no more a solution of the linear BFKL or DGLAP equations.

3.4 DGLAP evolution and the saturation boundary conditions[10]

One of the issues that could be studied in the context of the geometric scaling versus DGLAP evolution is the possibility of the different boundary conditions for the DGLAP evolution equations. These boundary conditions would incorporate the saturation effects and posses the scaling property. Typically, in the standard approach, to obtain the solution to the linear DGLAP evolution equations, one imposes the initial conditions onto the parton densities at fixed value of Q_0^2

[9] $\xi_1 \simeq -2.34$ is the rightmost zero of the Airy function.

[10] Contributing author: A. M. Stasto

and then performs the evolution into the region of larger values of Q^2. However, in the presence of saturation these might not be the correct boundary conditions for DGLAP equations. As mentioned earlier the saturation regime is specified by the critical line, the saturation scale $Q_s(x)$ which is a function of x Bjorken and its value increases as the Bjorken x decreases (or as we go to yet higher energies). In that case it seems legitimate to ask, what is the behavior of the DGLAP solutions when evolved from the saturation boundary $Q^2 = Q_s^2(x)$ rather then from the fixed scale $Q^2 = Q_0^2$. To answer this question we imposed [140] the boundary condition for the gluon density at the saturation scale $Q^2 = Q_s^2$ which possesses the scaling property namely $\frac{\alpha_s}{2\pi} x g(x, Q^2 = Q_s^2(x)) = \frac{\alpha_s}{2\pi} r^0 x^{-\lambda}$ (in the fixed coupling case). The solution for the gluon density at small x (at fixed coupling) which can be derived from solving the DGLAP equations with this boundary is given by

$$\frac{\alpha_s}{2\pi} \frac{x g(x, Q^2)}{Q^2} \sim \frac{\alpha_s}{2\pi} \left(\frac{Q^2}{Q_s^2(x)} \right)^{(\alpha_s/2\pi)\gamma_{gg}(\omega_0)-1} \tag{29}$$

where γ_{gg} is the gluon-gluon DGLAP anomalous dimension. This solution clearly has the geometrical scaling property as it is only a function of $Q^2/Q_s^2(x)$. It is interesting to note that there exists a critical value of the exponent λ of the saturation scale which determines the existence of scaling. For example in the double leading logarithmic approximation the scaling is present for rather large values of the exponent $\lambda \geq 4\alpha_s\pi/3$ whereas there is no scaling for smaller values of λ. The formula shown above is however only approximate, as in the derivation we included only the leading behavior which should be dominant at asymptotically small values of x. At any finite value of x the scaling will be mildly violated by the nonleading terms. We checked numerically that this is indeed the case, though the violation was very small. This analysis was extended for the case of the more realistic DGLAP evolution with the running coupling. As expected the presence of the scale violation due to the running coupling will lead to the violation of the scaling. In this case the geometric scaling is only approximate with the solution for the gluon density given by

$$\frac{\alpha_s(Q^2)}{2\pi} \frac{x g(x, Q^2)}{Q^2} \sim \frac{Q_s^2(x)}{Q^2} \left[1 + \frac{\alpha_s(Q_s^2(x))}{2\pi b} \ln[Q^2/Q_s^2(x)] \right]^{b\gamma_{gg}(\lambda)-1},$$

with b being the beta function of the QCD running coupling. The scaling here is present provided we have $\alpha_s(Q_s(x)) \ln[Q^2/Q_s^2(x)]/(2\pi b) \ll 1$. Thus the geometric scaling violating term can be factored out.

In summary, this analysis shows that the geometric scaling property can be build into the DGLAP initial conditions, and that the solution to the linear evolution equation which do not include the parton saturation effects can preserve the scaling even in the regime of high Q^2 values, outside the saturation region.

3.5 Geometric scaling from DGLAP evolution[11]

From the DGLAP point of view there is another possible explanation for geometric scaling: the scaling behaviour can be generated by the evolution itself, rather than being a preserved boundary condition. In fact, it is possible to show [141] both analytically and numerically that in

[11] Contributing author: F. Caola

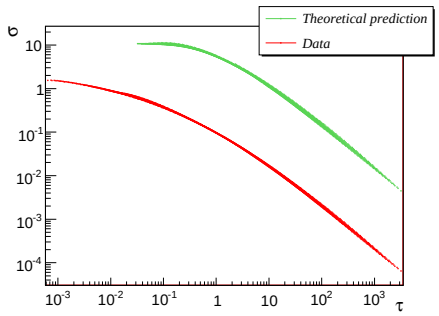

Fig. 18: Scaling plot with $x < 0.1$. For the theoretical DGLAP curve, only points with $Q^2 > 1$ GeV^2 were kept. Curves are offset for clarity.

the relevant HERA region approximate geometric scaling is a feature of the DGLAP evolution. In order to see this, one has first to rewrite the DGLAP solution as a function of $t-\lambda(t,x)\log 1/x$ ("fixed-coupling scaling") or $t-\lambda(t,x)\sqrt{\log 1/x}$ ("running-coupling scaling")[12] . Then from the explicit form of the DGLAP solution it follows that in the relevant kinematic region $\lambda(t,x)$ is approximatively constant, leading to $\sigma_{DGLAP}(t,x) \approx \sigma_{DGLAP}\left(t-t_s(x)\right)$. Hence approximate geometric scaling in the HERA region is a feature of the DGLAP evolution. Interestingly enough, this DGLAP-generated geometric scaling is expected to hold also at large Q^2 and relatively large x (say $x \lesssim 0.1$), in contrast with the saturation-based geometric scaling which should be a small x, small (or at least moderate) Q^2 effect.

In order to make more quantitative statements, one can use the quality factor method introduced in Sec. 3.2. As a starting point, one can consider the leading-order small x DGLAP evolution of a flat boundary condition. At the level of accuracy of geometric scaling, this approximation should be accurate enough in a wide kinematic region, say $Q^2 \gtrsim 10$ GeV^2, $x \lesssim 0.1$ at HERA. Now, a quality-factor analysis shows that in this region the leading-order small x DGLAP solution has an excellent scaling behaviour, even better than the scaling behaviour observed in HERA data. Also the DGLAP predictions for the geometric slope λ perfectly agree with the phenomenological values: from the DGLAP solution we obtain $\lambda_{fix}^{DGLAP} = 0.32 \pm 0.05$ ("fixed-coupling" scaling) and $\lambda_{run}^{DGLAP} = 1.66 \pm 0.34$ ("running-coupling" scaling), to be compared with $\lambda_{fix}^{exp} = 0.32 \pm 0.06$, $\lambda_{run}^{exp} = 1.62 \pm 0.25$. Moreover, data exhibit geometric scaling also for larger x, larger Q^2 (say $x \lesssim 0.1$ at HERA), as predicted by the DGLAP evolution. All these results are summarized in Fig. 18, where we plot the theoretical and phenomenological[13] reduced cross sections in function of the "fixed-coupling" scaling variable $\ln\tau = t - \lambda \ln 1/x$, with $\lambda = 0.32$, in the HERA region with the cut $x < 0.1$. An analogous plot can be obtained for the "running-coupling" scaling [141]. We interpret these results as striking evidence that for $Q^2 > 10$ GeV^2 the geometric scaling seen at HERA is generated by the DGLAP evolution itself,

[12] The labels "fixed-coupling" or "running-coupling" are here a bit misleading. In fact, all the results shown here are obtained with the full running-coupling DGLAP solution. We kept this notation only for comparison with saturation-based approaches.

[13] In fact, in order to make a more flexible analysis, we didn't use the actual HERA data but a neural network interpolation of world DIS data [142]. As long as one stays in the HERA region the output of the net is totally reliable.

without need of a peculiar saturation ansatz or of a suitable scaling boundary condition.

For $Q^2 < 10$ GeV^2 the leading-order DGLAP solution exhibits violations of geometric scaling at small x. However, in this region any fixed-order DGLAP calculation fails because it does not resum small x logarithms. If one consider the DGLAP evolution at the resummed level, geometric scaling reappears quite naturally, both in the "fixed-coupling" and "running-coupling" forms [141]. Hence, small x resummation extends the region where geometric scaling is expected to values of Q^2 lower than 10 GeV^2. However at low Q^2 sizeable higher twist and non perturbative effects can spoil the universal behaviour of the DGLAP solution. In this region hence the HERA scaling could still be generated by some DGLAP evolution, but, differently from the $Q^2 > 10$ GeV^2 region, here there is no strong evidence that this is in fact the case.

3.6 Saturation model and higher twists[14]

The QCD description of hard scattering processes within the Operator Product Expansion (OPE) approach leads to the twist expansion of matrix elements of process-dependent composite operators. Contributions of emerging local operators with the increasing twists, τ, are suppressed by increasing inverse powers of the hard scale, Q^2. In DIS, at the lowest order (i.e. when the anomalous dimensions vanish), the twist-τ contribution to the DIS cross section scales as $Q^{-\tau}$. Therefore, at sufficiently large Q^2 it is justified to neglect higher twist effects, and retain only the leading twist-2 contribution. This leads to the standard collinear factorisation approach with universal parton density functions evolving according to the DGLAP evolution equation. It should be kept in mind, however, that the higher twist effects do not vanish completely and that they introduce corrections to theoretical predictions based on the DGLAP approach. Thus, the higher twist corrections may affect the determination of parton density functions. The importance of these corrections depends on the level of precision required and on the kinematic domain. In particular, in the region of very small x the higher twist effects are expected to be enhanced, so that they may become significant at moderate Q^2. Thus, it should be useful to obtain reliable estimates of higher twist effects at small x. In this section we shall present higher twist corrections to F_T, F_L and F_2 structure functions following from the DGLAP improved saturation model [143]. The results presented in this section have been obtained in the course of an ongoing study [144, 145]. The method applied to perform the twist decomposition of the DGLAP improved saturation model is a generalisation of the Mellin space approach proposed in Ref. [146].

A rigorous QCD analysis of the higher twist contributions to DIS at high energies is a complex task. So far it has been performed for the $q\bar{q}gg$ operators [147], but the evolution of twist 4 purely gluonic operators has not been resolved, — even the proper complete basis of the operators has not been found yet. The collinear evolution is known at all twists, however, for so called *quasi-partonic operators*, for which the twist index is equal to the number of partons in the t-channel [148]. Such operators should receive the strongest enhancement from the QCD evolution. At the leading logarithmic approximation the collinear evolution of quasi-partonic operators is relatively simple — it is given by pair-wise interactions between the partons in the t-channel. The interactions are described by the non-forward DGLAP kernel [148]. Within this formalism, the evolution of four-gluon quasi-partonic operators was investigated in Ref. [149,

[14] Contributing author: L. Motyka

150] in the double logarithmic approximation. At small x the scattering amplitudes are driven by exchange of gluons in the t-channel, and the quark exchanges are suppressed by powers of x. Thus we shall focus on the dominant contribution of the multi-gluon exchanges in the t-channel. In the large N_c-limit, the dominant singularities of the four gluon operator are those corresponding to states in which gluons get paired into colour singlet states. In other words, the four-gluon operator evolves like a product of two independent gluon densities. In general, for $1/N_c \to 0$, the $2n$-gluon (twist-$2n$) operator factorizes into the product of n twist-2 gluon densities. After suitable inclusion of the AGK cutting rules and the symmetry factors of $1/n!$, one arrives at the eikonal picture of n-ladder exchange between the probe and the target. This is to be contrasted with the Balitsky-Kovchegov picture of Pomeron fan diagrams, which was obtained as a result of resummation of the terms enhanced by powers of large $\ln(1/x)$ rather than by powers of $\ln Q^2$.

The eikonal form of the multiple scattering was assumed in the saturation model proposed by Golec-Biernat and Wüsthoff (GBW) [151, 152]. The dipole cross-section given by Eq. 25 has a natural interpretation in terms of a resummation of multiple scattering amplitudes. The scatters are assumed to be independent of each other, and the contribution of n scatterings is proportional to $[r^2/R_0^2(x)]^n$. The connection of the saturation model to the QCD evolution of quasi-partonic operators is further strengthened by the DGLAP improvement of the dipole cross section [143]. In the DGLAP improved saturation model the dipole cross section depends on the collinear gluon density,

$$\hat{\sigma}(x,r) = \sigma_0 \left[1 - \exp\left(-\frac{\pi^2 r^2}{N_c \sigma_0} \alpha_s(\mu^2)\, x g(x,\mu^2) \right) \right], \tag{30}$$

where the scale μ^2 depends on the dipole size, $\mu^2 = C/r^2$ for $C/r^2 > \mu_0^2$, and $\mu^2 = \mu_0^2$ for $C/r^2 < \mu_0^2$. The gluon density applied has been obtained from the LO DGLAP evolution without quarks, with the input assumed at the scale μ_0^2 [15]. Clearly, in Eq. (30) one sees an exact matching between the power of r^2 and the power of $xg(x,\mu^2)$ suggesting a correspondence between the term $\sim [r^2 \alpha_s(\mu^2)\, x g(x,\mu^2)]^n$ in the expansion of $\hat{\sigma}(x,r)$ and the twist-$2n$ contribution to the dipole cross section. Thus, we expect that the saturation model approximately represents higher twist contributions in the deep inelastic scattering generated by the gluonic quasi-partonic operators.

The twist analysis of the DIS cross-section must include a treatment of the quark box that mediates the coupling of the virtual photon, γ^*, to the t-channel gluons. In the dipole model the $\gamma^* g \to q\bar{q}$ amplitude, computed within QCD, is Fourier transformed (w.r.t. the transverse momentum of the quark) to the coordinate representation and appears as the photon wave function, compare Eq. (25). In more detail, one uses the $\gamma^* g$ amplitude computed within the k_T-factorisation framework. This amplitude receives contributions from all twists. The twist structure of the quark box is transparent in the space of Mellin moments, and the same is true for the dipole cross-section. Thus we define,

$$\tilde{H}_{T,L}(\gamma, Q^2) = \int_0^1 dz \int_0^\infty dr^2\; r^2 \left| \Psi_{T,L}(r,z,Q^2) \right|^2 \; r^{2(\gamma-1)}\,, \tag{31}$$

[15] In the original DGLAP-improved model [143] a different definition of the scale was adopted, $\mu^2 = C/r^2 + \mu_0^2$, but this choice is less convenient for the QCD analysis.

$$\tilde{\hat{\sigma}}(x,\gamma) = \int_0^\infty dr^2\, \hat{\sigma}(x,r^2)\, r^{2(\gamma-1)}\,. \tag{32}$$

It then follows from the Parsival formula that,

$$\sigma_{T,L}(x,Q^2) = \int_{\mathcal{C}} \frac{d\gamma}{2\pi i}\, \tilde{H}_{T,L}(-\gamma,Q^2)\, \tilde{\hat{\sigma}}(x,\gamma). \tag{33}$$

For the massless quark case one has $\tilde{H}_{T,L}(\gamma,Q^2) = \tilde{H}_{T,L}(\gamma)\, Q^{-2\gamma}$. The contour of integration, $\mathcal{C}$, in Eq. 33 belongs to the fundamental Mellin strip, $-1 < \mathrm{Re}\,\gamma < 0$.

In order to obtain the twist expansion of σ, one extends the contour $\mathcal{C}$ in the complex γ-plane into a contour $\mathcal{C}'$ closed from the left-hand side. The Mellin integral in Eq. 33 may be then decomposed into contributions coming from singularities of $\tilde{H}_{T,L}(-\gamma,Q^2)\, \tilde{\hat{\sigma}}(x,\gamma)$. The function $\tilde{H}_T(-\gamma)$ ($\tilde{H}_L(-\gamma)$) has simple poles at all negative integer values of γ, except of $\gamma = -2$ ($\gamma = -1$), where $\tilde{H}_T$ ($\tilde{H}_L$) is regular. The singularity structure of the dipole cross section, $\tilde{\hat{\sigma}}(\gamma)$, depends on the specific form of $\hat{\sigma}(x,r^2)$. For $\hat{\sigma}(x,r^2)$ used in the GBW model, the $\tilde{\hat{\sigma}}(x,\gamma)$ has simple poles at all negative integers γ's. For the DGLAP improved form of $\hat{\sigma}$ given by (31), $\tilde{\hat{\sigma}}(x,\gamma)$ has cut singularities that extend to the left from $\gamma = k$ where $k = -1, -2,$ etc. The leading behaviour of $\tilde{\hat{\sigma}}$ around a branch point at $\gamma = k$ is given by $\sim (\gamma - k)^{p(k)}$, where the exponent $p(k)$ is generated by the DGLAP evolution. As the cuts extend to the left from the branch points, the dominant contribution to the cross section at the given twist comes from the vicinity of the corresponding branch point.

The singularity structure of the quark box part $\tilde{H}_{T,L}(\gamma)$ plays the crucial role in understanding the strength of the subleading twist effects. To see that one expands $\tilde{H}_{T,L}(\gamma)$ around the singular points, $\gamma = 1$ and $\gamma = 2$ (recall that the argument of $\tilde{H}_{T,L}$ is $-\gamma$ in the Parsival formula (33)):

$$\tilde{H}_T(\gamma) = \frac{a_T^{(2)}}{\gamma - 1} + b_T^{(2)} + \mathcal{O}(\gamma - 1), \qquad H_L(\gamma) = b_L^{(2)} + \mathcal{O}(\gamma - 1), \tag{34}$$

for twist-2, and

$$\tilde{H}_T(\gamma) = b_T^{(4)} + \mathcal{O}(\gamma - 2), \qquad H_L(\gamma) = \frac{a_L^{(4)}}{\gamma - 2} + b_L^{(4)} + \mathcal{O}(\gamma - 2), \tag{35}$$

for twist-4. The singular $1/(\gamma - 1)$ and $1/(\gamma - 2)$ terms in (34) and (35) generate an additional enhancement, $\sim \ln(Q^2)$, of the corresponding twist-2 and twist-4 contributions to the DIS cross-section. The constant pieces, proportional to $b_{T,L}^{(2)}$ and $b_{T,L}^{(4)}$, produce no new logarithms (thus they are interpreted as the next-to-leading order (NLO) QCD corrections) and the higher terms in the Laurent expansion give yet higher orders in the perturbative expansion of the $g \to q$ splitting functions and to the coefficient functions. We summarize this discussion by displaying below the most leading contributions to $\sigma_{T,L}$ at twist-2 ($\sigma_{T,L}^{(2)}$) and at twist-4 ($\sigma_{T,L}^{(4)}$) obtained in the DGLAP improved saturation model:

$$\sigma_T^{(2)} \;\sim\; \frac{a_T^{(2)}}{Q^2} \int_{\mu_0^2}^{Q^2} \frac{dQ'^2}{Q'^2} \alpha_s(Q'^2) x g(x,Q'^2)\,, \qquad \sigma_L^{(2)} \;\sim\; \frac{b_L^{(2)}}{Q^2}\, \alpha_s(Q^2) x g(x,Q^2)\,, \tag{36}$$

for twist-2, and

$$\sigma_T^{(4)} \sim \frac{b_T^{(4)}}{Q^4}[\alpha_s(Q^2)xg(x,Q^2)]^2\,, \qquad \sigma_L^{(4)} \sim \frac{a_L^{(4)}}{Q^4}\int_{\mu_0^2}^{Q^2}\frac{dQ'^2}{Q'^2}[\alpha_s(Q'^2)xg(x,Q'^2)]^2\,, \quad (37)$$

for twist-4. These results imply that the the relative twist-4 correction to F_T is strongly suppressed w.r.t. the twist-2 contribution, as the subleading twist-4 term in F_T appears only at the NLO. On the contrary, for F_L, the leading twist term enters only at the NLO, and the the twist-4 correction enters at the leading order. So, the relative twist-4 effects in F_L are expected to be enhanced. Note, that both in the case of F_T and F_L the twist-4 effects are enhanced w.r.t. the twist-2 contribution by an additional power of the gluon density, $xg(x,Q^2)$. For the structure function $F_2 = F_T + F_L$ we expect small relative corrections from the higher twists because of the opposite sign of coefficients $a_L^{(4)}$ and $b_T^{(4)}$, that leads to cancellations between the twist-4 contributions from F_T and F_L at moderate Q^2. These conclusions about the importance of the higher twist corrections are expected to be quite general, because they follow directly from the twist structure of the quark box and do not depend on the detailed form of the twist-4 gluon distribution.

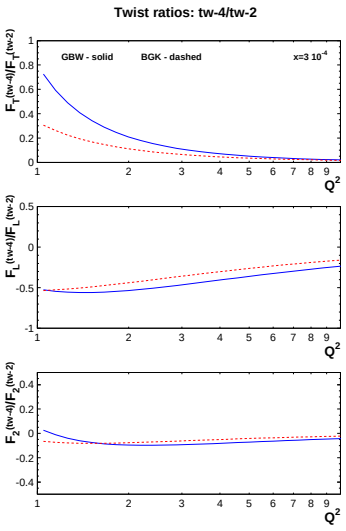

Fig. 19: The ratio of twist-4 to twist-2 components of F_T, F_L and F_2 at $x = 3\cdot 10^{-4}$ in the GBW model (continuous lines) and in the DGLAP improved saturation model (dashed lines).

We performed [144, 145] an explicit numerical evaluation of the twist-4 corrections to F_T, F_L and F_2 in the DGLAP improved saturation model, and compared the results to results obtained [146] within the GBW model without the DGLAP evolution. The parameters of the DGLAP model were fitted to describe all F_2 data at small x. In the model we took into account three massless quark flavours and the massive charm quark. The twist analysis, however, has been, so far, performed only for the massless quark contribution. The obtained relative twist-4 corrections to F_T, F_L and F_2 are displayed in Fig. 3.6, as a function of Q^2, for $x = 3\cdot 10^{-4}$. The continuous curves correspond to the GBW model [146], and the dashed ones have been obtained [144, 145] in the DGLAP improved saturation model. Although there are some quantitative differences between the models, the qualitative picture is quite consistent and confirms the results of the analytic analysis outlined above. Thus, the higher twist corrections are strongest in F_L, and much weaker in F_T. In F_2 there occurs a rather fine cancellation between the twist-4 contributions to F_T and F_L, at all Q^2, down to 1 GeV^2. Although an effect of this kind was expected, it still remains somewhat surprising that this cancellation works so well. We estimate that, for $x = 3\cdot 10^{-4}$, the twist-4 relative correction to F_2 is $2-4\%$ at $Q^2 = 10$ GeV^2, and smaller than 10% for all Q^2 down to 1 GeV^2. For F_L, the relative correction is $\sim 20\%$ at $Q^2 = 10$ GeV^2, and strongly increases with the decreasing scale, reaching $\sim 50\%$ at $Q^2 = 1$ GeV^2. It implies that the determination of parton densities from twist-2 F_2 data is

safe even at small x and moderate Q^2. On the other hand F_L at small x may provide a sensitive probe of higher twist effects and parton saturation.

3.7 Conclusions

There are many possible explanations for the scaling properties of HERA data, some of them based on saturation effects and some others based on pure linear evolution. In order to separate between these different explanations, it is fundamental to specify a kinematic window.

In particular, for large enough Q^2 and not too small x (say $Q^2 \gtrsim 10$ GeV^2 in the HERA region) the observed geometric scaling is determined by the DGLAP evolution, irrespective of the boundary condition. For smaller values of Q^2, the evolution of parton densities is still linear, but is sensitive to a boundary condition. In an evolution toward smaller x, like BFKL, this boundary condition is dynamically generated by saturation, and it leads to the geometric scaling window. It is possible to take these effects into account also in a Q^2 evolution, like DGLAP, by imposing as initial condition the same boundary condition. We have seen that, in this case, even the LO DGLAP equation is able to propagate geometric scaling towards larger Q^2. In that domain, although geometric scaling may arise as saturation effect, the evolution is still linear, and thus compatible with standard PDFs analysis. However, at yet lower Q^2 and x standard linear evolution is no longer reliable. In particular, for Q^2 smaller than a x dependent saturation scale $Q_s(x)$, the evolution of parton densities becomes fully nonlinear, and this spoils the actual determination of the PDFs. Results from inclusive diffraction and vector meson exclusive production at HERA, and from dA collisions at RHIC all suggest that in the kinematic accessible x region $Q_s \sim 1 - 2$ GeV.

In conclusion, we can say that for large enough $Q^2 \gtrsim 10$ GeV^2 geometric scaling is fully compatible with linear DGLAP evolution. For smaller Q^2 the situation becomes more involved. For $Q^2 \gtrsim 5$ GeV^2 the HERA scaling is still compatible with DGLAP, maybe with some small x resummation or some suitable boundary condition. However, other effects may be relevant in this region. For yet lower Q^2 and x the linear theory becomes unreliable and saturation could be the right explanation for geometric scaling. Unfortunately at HERA we have too few data for a definitive explanation of geometric scaling in the very small x region, since many different approaches lead approximatively to the same results and it is very difficult to separate among them. For example, in the low x region both saturation and perturbative resummations lead to a decrease of the gluon and to geometric scaling. At the LHC, where higher center-of-mass energy is available, the x region is significantly extended down to very small values. Especially in the fragmentation region the typical values of x which can be probed can reach down to 10^{-6} for partons with transverse momenta of about few GeV. This fact combined with the very wide rapidity coverage of the main LHC detectors opens up a completely new window for the study of parton saturation, and its relations with geometric scaling and linear evolution will possibly be clarified.

References

[1] S. A. Larin, T. van Ritbergen, and J. A. M. Vermaseren, Nucl. Phys. **B427**, 41 (1994).

[2] S. A. Larin, P. Nogueira, T. van Ritbergen, and J. A. M. Vermaseren, Nucl. Phys. **B492**, 338 (1997). hep-ph/9605317.

[3] A. Retey and J. A. M. Vermaseren, Nucl. Phys. **B604**, 281 (2001). hep-ph/0007294.

[4] S. Moch, J. A. M. Vermaseren, and A. Vogt, Nucl. Phys. **B688**, 101 (2004). hep-ph/0403192.

[5] A. Vogt, S. Moch, and J. A. M. Vermaseren, Nucl. Phys. **B691**, 129 (2004). hep-ph/0404111.

[6] S. Moch, J. A. M. Vermaseren, and A. Vogt, Phys. Lett. **B606**, 123 (2005). hep-ph/0411112.

[7] J. A. M. Vermaseren, A. Vogt, and S. Moch, Nucl. Phys. **B724**, 3 (2005). hep-ph/0504242.

[8] A. Vogt, S. Moch, and J. Vermaseren, Nucl. Phys. Proc. Suppl. **160**, 44 (2006). hep-ph/0608307.

[9] S. Moch and M. Rogal, Nucl. Phys. **B782**, 51 (2007). 0704.1740.

[10] S. Moch, M. Rogal, and A. Vogt, Nucl. Phys. **B790**, 317 (2008). 0708.3731.

[11] A. Vogt, S. Moch, M. Rogal, and J. A. M. Vermaseren, Nucl. Phys. Proc. Suppl. **183**, 155 (2008). 0807.1238.

[12] S. Moch, M. Rogal, A. Vogt, and J. Vermaseren. In preparation.

[13] Particle Data Group Collaboration, W. M. Yao *et al.*, J. Phys. **G33**, 1 (2006).

[14] CCFR/NuTeV Collaboration, U.-K. Yang *et al.*, Phys. Rev. Lett. **86**, 2742 (2001). hep-ex/0009041.

[15] NuTeV Collaboration, M. Tzanov *et al.*, Phys. Rev. **D74**, 012008 (2006). hep-ex/0509010.

[16] CHORUS Collaboration, G. Onengut *et al.*, Phys. Lett. **B632**, 65 (2006).

[17] H1 Collaboration, C. Adloff *et al.*, Eur. Phys. J. **C30**, 1 (2003). hep-ex/0304003.

[18] ZEUS Collaboration, S. Chekanov *et al.*, Eur. Phys. J. **C32**, 1 (2003). hep-ex/0307043.

[19] H1 Collaboration, A. Aktas *et al.*, Phys. Lett. **B634**, 173 (2006). hep-ex/0512060.

[20] ZEUS Collaboration, S. Chekanov *et al.*, Phys. Lett. **B637**, 210 (2006). hep-ex/0602026.

[21] M. L. Mangano *et al.*, *Physics at the front-end of a neutrino factory: A quantitative appraisal*. Preprint hep-ph/0105155, 2001.

[22] J. B. Dainton, M. Klein, P. Newman, E. Perez, and F. Willeke, JINST **1**, P10001 (2006). hep-ex/0603016.

[23] NuTeV Collaboration, G. P. Zeller *et al.*, Phys. Rev. Lett. **88**, 091802 (2002). hep-ex/0110059.

[24] H1 Collaboration, A. Aktas *et al.*, Phys. Lett. **B632**, 35 (2006). hep-ex/0507080.

[25] S. Davidson, S. Forte, P. Gambino, N. Rius, and A. Strumia, JHEP **02**, 037 (2002). hep-ph/0112302.

[26] K. S. McFarland and S.-O. Moch, *Conventional physics explanations for the NuTeV sin**2(theta(W))*. Preprint hep-ph/0306052, 2003.

[27] B. A. Dobrescu and R. K. Ellis, Phys. Rev. **D69**, 114014 (2004). hep-ph/0310154.

[28] S. Kretzer *et al.*, Phys. Rev. Lett. **93**, 041802 (2004). hep-ph/0312322.

[29] A. J. Buras, Rev. Mod. Phys. **52**, 199 (1980).

[30] S. G. Gorishnii, S. A. Larin, L. R. Surguladze, and F. V. Tkachov, Comput. Phys. Commun. **55**, 381 (1989).

[31] S. A. Larin, F. V. Tkachov, and J. A. M. Vermaseren. NIKHEF-H-91-18.

[32] D. J. Broadhurst, A. L. Kataev, and C. J. Maxwell, Phys. Lett. **B590**, 76 (2004). hep-ph/0403037.

[33] W. L. van Neerven and A. Vogt, Nucl. Phys. **B603**, 42 (2001). hep-ph/0103123.

[34] E. A. Paschos and L. Wolfenstein, Phys. Rev. **D7**, 91 (1973).

[35] S. Moch, J. A. M. Vermaseren, and A. Vogt, Nucl. Phys. **B726**, 317 (2005). hep-ph/0506288.

[36] S. Catani, D. de Florian, G. Rodrigo, and W. Vogelsang, Phys. Rev. Lett. **93**, 152003 (2004). hep-ph/0404240.

[37] H. L. Lai *et al.*, JHEP **04**, 089 (2007). hep-ph/0702268.

[38] R. S. Thorne, A. D. Martin, W. J. Stirling, and G. Watt, *Parton Distributions for the LHC*. Preprint 0706.0456, 2007.

[39] A. Vogt (2007). arXiv:0707.4106.

[40] V. S. Fadin, E. A. Kuraev, and L. N. Lipatov, Phys. Lett. **B60**, 50 (1975).

[41] I. I. Balitsky and L. N. Lipatov, Sov. J. Nucl. Phys. **28**, 822 (1978).

[42] V. S. Fadin and L. N. Lipatov, Phys. Lett. **B429**, 127 (1998). hep-ph/9802290.

[43] G. Camici and M. Ciafaloni, Phys. Lett. **B412**, 396 (1997). hep-ph/9707390.

[44] M. Ciafaloni and G. Camici, Phys. Lett. **B430**, 349 (1998). hep-ph/9803389.

[45] S. Marzani, R. D. Ball, P. Falgari, and S. Forte, Nucl. Phys. **B783**, 143 (2007). 0704.2404.

[46] M. Ciafaloni, D. Colferai, D. Colferai, G. P. Salam, and A. M. Stasto, Phys. Lett. **B576**, 143 (2003). hep-ph/0305254.

[47] M. Ciafaloni, D. Colferai, G. P. Salam, and A. M. Stasto, Phys. Rev. **D68**, 114003 (2003). hep-ph/0307188.

[48] S. Catani, M. Ciafaloni, and F. Hautmann, Nucl. Phys. **B366**, 135 (1991).

[49] S. Catani and F. Hautmann, Nucl. Phys. **B427**, 475 (1994). hep-ph/9405388.

[50] A. Bialas, H. Navelet, and R. B. Peschanski, Nucl. Phys. **B603**, 218 (2001). hep-ph/0101179.

[51] C. D. White, R. B. Peschanski, and R. S. Thorne, Phys. Lett. **B639**, 652 (2006). hep-ph/0606169.

[52] G. Altarelli, R. D. Ball, and S. Forte, Nucl. Phys. **B575**, 313 (2000). hep-ph/9911273.

[53] G. Altarelli, R. D. Ball, and S. Forte, Nucl. Phys. **B621**, 359 (2002). hep-ph/0109178.

[54] G. Altarelli, R. D. Ball, and S. Forte, Nucl. Phys. **B674**, 459 (2003). hep-ph/0306156.

[55] G. Altarelli, R. D. Ball, and S. Forte, Nucl. Phys. **B742**, 1 (2006). hep-ph/0512237.

[56] R. D. Ball and S. Forte, Nucl. Phys. **B742**, 158 (2006). hep-ph/0601049.

[57] R. D. Ball, Nucl. Phys. **B796**, 137 (2008). 0708.1277.

[58] G. Altarelli, R. D. Ball, and S. Forte, Nucl. Phys. **B799**, 199 (2008). 0802.0032.

[59] G. Altarelli, R. D. Ball, and S. Forte, *Structure Function Resummation in small-x QCD*. Preprint 0802.0968, 2007.

[60] G. P. Salam, JHEP **07**, 019 (1998). hep-ph/9806482.

[61] M. Ciafaloni and D. Colferai, Phys. Lett. **B452**, 372 (1999). hep-ph/9812366.

[62] M. Ciafaloni, D. Colferai, and G. P. Salam, Phys. Rev. **D60**, 114036 (1999). hep-ph/9905566.

[63] M. Ciafaloni, D. Colferai, and G. P. Salam, JHEP **07**, 054 (2000). hep-ph/0007240.

[64] M. Ciafaloni and D. Colferai, JHEP **09**, 069 (2005). hep-ph/0507106.

[65] M. Ciafaloni, D. Colferai, G. P. Salam, and A. M. Stasto, Phys. Lett. **B635**, 320 (2006). hep-ph/0601200.

[66] M. Ciafaloni, D. Colferai, G. P. Salam, and A. M. Stasto, JHEP **08**, 046 (2007). 0707.1453.

[67] R. S. Thorne, Phys. Rev. **D60**, 054031 (1999). hep-ph/9901331.

[68] R. S. Thorne, Nucl. Phys. Proc. Suppl. **79**, 210 (1999). hep-ph/9906323.

[69] R. S. Thorne, Phys. Lett. **B474**, 372 (2000). hep-ph/9912284.

[70] R. S. Thorne, Phys. Rev. **D64**, 074005 (2001). hep-ph/0103210.

[71] C. D. White and R. S. Thorne, Phys. Rev. **D74**, 014002 (2006). hep-ph/0603030.

[72] C. D. White and R. S. Thorne, Phys. Rev. **D75**, 034005 (2007). hep-ph/0611204.

[73] M. Dittmar *et al.*, *Parton distributions: Summary report for the HERA - LHC workshop*. Preprint hep-ph/0511119, 2005.

[74] R. D. Ball and S. Forte, Phys. Lett. **B465**, 271 (1999). hep-ph/9906222.

[75] G. Altarelli, R. D. Ball, and S. Forte, Nucl. Phys. **B599**, 383 (2001). hep-ph/0011270.

[76] G. Altarelli, R. D. Ball, and S. Forte, *An improved splitting function for small x evolution*. Preprint hep-ph/0310016, 2003.

[77] G. Altarelli, R. D. Ball, and S. Forte, Nucl. Phys. Proc. Suppl. **135**, 163 (2004). hep-ph/0407153.

[78] R. D. Ball and S. Forte, Phys. Lett. **B405**, 317 (1997). hep-ph/9703417.

[79] L. Lipatov, Sov. Phys. JETP **5**, 5 (1986).

[80] R. D. Ball and R. K. Ellis, JHEP **05**, 053 (2001). hep-ph/0101199.

[81] B. Andersson, G. Gustafson, H. Kharraziha, and J. Samuelsson, Z. Phys. **C71**, 613 (1996).

[82] J. Kwiecinski, A. D. Martin, and P. J. Sutton, Z. Phys. **C71**, 585 (1996). hep-ph/9602320.

[83] J. Kwiecinski, A. D. Martin, and A. M. Stasto, Phys. Rev. **D56**, 3991 (1997). hep-ph/9703445.

[84] J. C. Collins and J. Kwiecinski, Nucl. Phys. **B316**, 307 (1989).

[85] C. D. White and R. S. Thorne, Eur. Phys. J. **C45**, 179 (2006). hep-ph/0507244.

[86] D0 Collaboration, B. Abbott *et al.*, Phys. Rev. Lett. **86**, 1707 (2001). hep-ex/0011036.

[87] CDF Collaboration, T. Affolder *et al.*, Phys. Rev. **D64**, 032001 (2001). hep-ph/0102074.

[88] H1 Collaboration, C. Adloff *et al.*, Eur. Phys. J. **C19**, 269 (2001). hep-ex/0012052.

[89] H1 Collaboration, C. Adloff *et al.*, Eur. Phys. J. **C21**, 33 (2001). hep-ex/0012053.

[90] ZEUS Collaboration, J. Breitweg *et al.*, Eur. Phys. J. **C7**, 609 (1999). hep-ex/9809005.

[91] ZEUS Collaboration, S. Chekanov *et al.*, Eur. Phys. J. **C21**, 443 (2001). hep-ex/0105090.

[92] A. D. Martin, W. J. Stirling, and R. S. Thorne, Phys. Lett. **B635**, 305 (2006). hep-ph/0601247.

[93] R. S. Thorne, Phys. Rev. **D73**, 054019 (2006). hep-ph/0601245.

[94] H1 Collaboration, F. D. Aaron *et al.*, Phys. Lett. **B665**, 139 (2008). 0805.2809.

[95] A. D. Martin, W. J. Stirling, R. S. Thorne, and G. Watt, Phys. Lett. **B652**, 292 (2007). 0706.0459.

[96] M. Ciafaloni, Phys. Lett. **B356**, 74 (1995). hep-ph/9507307.

[97] M. Diemoz, F. Ferroni, E. Longo, and G. Martinelli, Z. Phys. **C39**, 21 (1988).

[98] R. D. Ball and S. Forte, Phys. Lett. **B359**, 362 (1995). hep-ph/9507321.

[99] P. F. R. *Photon–Hadron Interactions*. Benjamin, New York, 1972.

[100] Bjorken, J.D., Lecture Notes in Physics, **56**, Springer, Berlin (1976).

[101] Kuraev, E.A. and Lipatov, L.N. and Fadin, V.S., Sov. Phys. JETP **45**, 199 (1977).

[102] N. G. V. and N. L. L. Sov. J. Nucl. Phys. **15**, 438 (1972).

[103] N. G. V. and N. L. L. Sov. J. Nucl. Phys. **15**, 675 (1972).

[104] G. Altarelli and G. Parisi, Nucl. Phys. **B 126**, 298 (1977).

[105] L. D. Yu. Sov. Phys. JETP **46**, 641 (1977).

[106] Gribov, L.V. and Levin, E.M. and Ryskin, M.G., Phys. Rept. **100**, 1 (1983).

[107] Mueller, A.H., Nucl. Phys. **B558**, 285 (1999).

[108] E. Iancu and R. Venugopalan, *The color glass condensate and high energy scattering in QCD*. Preprint hep-ph/0303204, 2003.

[109] Balitsky, I., Nucl. Phys. **B463**, 99 (1996).

[110] Kovchegov, Yu.V., Phys. Rev. **D61**, 074018 (2000).

[111] A. M. Stasto, K. J. Golec-Biernat, and J. Kwiecinski, Phys. Rev. Lett. **86**, 596 (2001). hep-ph/0007192.

[112] S. Munier and R. Peschanski, Phys. Rev. **D69**, 034008 (2004). hep-ph/0310357.

[113] F. Gelis, R. B. Peschanski, G. Soyez, and L. Schoeffel, Phys. Lett. **B647**, 376 (2007). hep-ph/0610435.

[114] ZEUS Collaboration, J. Breitweg *et al.*, Phys. Lett. **B487**, 273 (2000). hep-ex/0006013.

[115] ZEUS Collaboration, S. Chekanov *et al.*, Phys. Rev. **D70**, 052001 (2004). hep-ex/0401003.

[116] New Muon Collaboration Collaboration, M. Arneodo *et al.*, Nucl. Phys. **B483**, 3 (1997). hep-ph/9610231.

[117] E665 Collaboration, M. R. Adams *et al.*, Phys. Rev. **D54**, 3006 (1996).

[118] G. Beuf, R. Peschanski, C. Royon, and D. Salek, *Systematic Analysis of Scaling Properties in Deep Inelastic Scattering*. Preprint arXiv:0803.2186 [hep-ph], 2008.

[119] H1 Collaboration, F. D. Aaron *et al.*, Phys. Lett. **B659**, 796 (2008). 0709.4114.

[120] H1 Collaboration, A. Aktas *et al.*, Eur. Phys. J. **C44**, 1 (2005). hep-ex/0505061.

[121] H1 Collaboration, A. Aktas *et al.*, Eur. Phys. J. **C48**, 715 (2006). hep-ex/0606004.

[122] ZEUS Collaboration, S. Chekanov *et al.*, Nucl. Phys. **B713**, 3 (2005). hep-ex/0501060.

[123] ZEUS Collaboration, S. Chekanov *et al.*, Eur. Phys. J. **C38**, 43 (2004). hep-ex/0408009.

[124] ZEUS Collaboration, S. Chekanov *et al.*, Nucl. Phys. **B718**, 3 (2005). hep-ex/0504010.

[125] H1 Collaboration, A. Aktas *et al.*, Eur. Phys. J. **C46**, 585 (2006). hep-ex/0510016.

[126] H1 Collaboration, C. Adloff *et al.*, Eur. Phys. J. **C13**, 371 (2000). hep-ex/9902019.

[127] H1 Collaboration, C. Adloff *et al.*, Z. Phys. **C72**, 593 (1996). hep-ex/9607012.

[128] H1 Collaboration, C. Adloff *et al.*, Phys. Lett. **B528**, 199 (2002). hep-ex/0108039.

[129] ZEUS Collaboration, J. Breitweg *et al.*, Phys. Lett. **B407**, 402 (1997). hep-ex/9706009.

[130] European Muon Collaboration, J. J. Aubert *et al.*, Nucl. Phys. **B213**, 31 (1983).

[131] P. M. Nadolsky *et al.*, Phys. Rev. **D78**, 013004 (2008). 0802.0007.

[132] A. D. Martin, R. G. Roberts, W. J. Stirling, and R. S. Thorne, Phys. Lett. **B604**, 61 (2004). hep-ph/0410230.

[133] M. Gluck, E. Reya, and A. Vogt, Eur. Phys. J. **C5**, 461 (1998). hep-ph/9806404.

[134] R. C. Beuf, G. and D. Salek, to appear.

[135] E. Iancu, K. Itakura, and L. McLerran, Nucl. Phys. **A708**, 327 (2002). hep-ph/0203137.

[136] A. H. Mueller and D. N. Triantafyllopoulos, Nucl. Phys. **B640**, 331 (2002). hep-ph/0205167.

[137] E. Gardi, J. Kuokkanen, K. Rummukainen, and H. Weigert, Nucl. Phys. **A784**, 282 (2007). hep-ph/0609087.

[138] J. L. Albacete and Y. V. Kovchegov, Phys. Rev. **D75**, 125021 (2007). arXiv:0704.0612 [hep-ph].

[139] G. Beuf, *An alternative scaling solution for high-energy qcd saturation with running coupling*. Preprint arXiv:0803.2167 [hep-ph], 2008.

[140] J. Kwiecinski and A. M. Stasto, Phys. Rev. **D66**, 014013 (2002). hep-ph/0203030.

[141] F. Caola and S. Forte, Phys. Rev. Lett. **101**, 022001 (2008). 0802.1878.

[142] NNPDF Collaboration, L. Del Debbio, S. Forte, J. I. Latorre, A. Piccione, and J. Rojo, JHEP **03**, 080 (2005). hep-ph/0501067.

[143] J. Bartels, K. J. Golec-Biernat, and H. Kowalski, Phys. Rev. **D66**, 014001 (2002). hep-ph/0203258.

[144] K. G.-B. J. Bartels and L. Motyka, *in preparation*.

[145] L. Motyka, *Higher twists from the saturation model*. Talk at the 4th HERA and the LHC workshop, CERN, 26–30 May 2008, http://indico.cern.ch/conferenceDisplay.py?confId=27458.

[146] J. Bartels, K. J. Golec-Biernat, and K. Peters, Eur. Phys. J. **C17**, 121 (2000). hep-ph/0003042.

[147] R. K. Ellis, W. Furmanski, and R. Petronzio, Nucl. Phys. **B212**, 29 (1983).

[148] A. P. Bukhvostov, G. V. Frolov, L. N. Lipatov, and E. A. Kuraev, Nucl. Phys. **B258**, 601 (1985).

[149] J. Bartels and M. G. Ryskin, Z. Phys. **C60**, 751 (1993).

[150] J. Bartels and M. G. Ryskin, Z. Phys. **C62**, 425 (1994).

[151] K. J. Golec-Biernat and M. Wusthoff, Phys. Rev. **D59**, 014017 (1999). hep-ph/9807513.

[152] K. J. Golec-Biernat and M. Wusthoff, Phys. Rev. **D60**, 114023 (1999). hep-ph/9903358.